JACS
JOURNAL OF THE AMERICAN CHEMICAL SOCIETY

Perspective

pubs.acs.org/JACS

Bioinspired Interfaces with Superwettability: From Materials to Chemistry

Bin Su,[‖] Ye Tian,[‡] and Lei Jiang*[,†,§,‖]

[†]Laboratory of Bioinspired Smart Interfacial Science, Technical Institute of Physics and Chemistry, Chinese Academy of Sciences, Beijing 100190, P. R. China

[‡]Beijing National Laboratory for Molecular Sciences, Key Laboratory of Organic Solids, Institute of Chemistry, Chinese Academy of Sciences, Beijing 100190, P. R. China

[§]School of Chemistry and Environment, Beihang University, Beijing 100191, P. R. China

[‖]Department of Chemical Engineering, Monash University, Clayton, Victoria 3800, Australia

ABSTRACT: Superwettability is a special case of the wetting phenomenon among liquids, gases, and solids. The superhydrophobic/superhydrophilic effect discovered initially has undergone a century of development based on materials science and biomimetics. With the rapid development of research on anti-wetting materials, superoleophobic/superoleophilic surfaces have been fabricated to repel organic liquids besides water. Further studies of underwater superoleophobic/superoleophilic/superaerophobic/superaerophilic materials provide an alternative way to fabricate anti-wetting surfaces rather than lowering the surface energy. Owing to a series of efforts on the studying of extreme wettabilities, a mature superwettability system gradually evolved and has since become a vibrant area of active research, covering topics of superhydrophobicity/superhydrophilicity, superoleophobicity/superoleophilicity in gas or under liquid, superaerophobicity/superaerophilicity under liquid, and combinations of these states. The kinetic study of the superwettability system includes statics and dynamics, while the studied material structures range from traditional two-dimensional materials to three-dimensional, one-dimensional, and zero-dimensional materials. Furthermore, the wetting liquids range from water to oil, aqueous solutions, and ionic liquids, as well as liquid crystals and other types of liquids. The wetting conditions extend over a wide range of temperatures, pressures, and other external fields. With the development of this series of research, many new theories and functional interfacial materials have been fabricated, including self-cleaning textiles, oil/water separation systems, and water collection systems, and some of these have already been applied in industry. Moreover, the study of superwettability has also introduced many new phenomena and principles to the field of interfacial chemistry that display its vast potential in both materials and chemistry. The present Perspective aims to summarize the most recent research on these materials and their interfacial chemistry. An overview of novel materials in superwettability systems and interfacial materials is presented. Specifically, the evolution of superwettable materials will be introduced, and the fundamental rules for building these superwetting materials will be discussed, followed by a summary of recent progress in the application of superwettable materials to alter the behaviors of chemical reactants and products. Specific emphasis is placed on recent strategies that exploit superwettable materials to influence the performance of traditional chemical reactions and their unique contributions to chemistry, including the effective collection of reaction products, unique growth models of precipitates, and a simple strategy for the alignment/assembly of nanoscale building blocks. Finally, a short perspective is provided on the potential for future developments in the field.

continued...

1. INTRODUCTION

Wetting is a common phenomenon that can be widely observed anywhere from high tides on the beach to ion channels in cell membranes. Wetting can be defined as the ability of a liquid to maintain contact with a solid surface and is determined by the intermolecular interactions between the two phases.[1−3] Research on wetting and wettability has been an area of study for over two hundred years, beginning with the introduction of Young's equation in 1805.[4] After the fundamentals of wettability and a framework to study this phenomenon were established, several primary experimental discoveries were made. For example, Coghill and Anderson reported an anti-wetting soot/lycopodium mixture in 1907.[5,6] In 1953, Bartell and Shepard found that microscale pyramid-shaped paraffin surfaces exhibited an excellent water repellency (Figure 1a).[7] In 2001, Jiang et al. reported that nanoscale vertically aligned carbon nanotube films exhibited a superamphiphobic (i.e., both superhydrophobic and superoleophobic) property (Figure 1b), indicating the importance of nanostructures in building anti-wetting surfaces.[8] Then, a number of materials with superwettability have been developed through either "bottom-up"[9] or "top-down"[10,11] methods.

From the biomimetic approach, looking to examples of superwettable or super-water-repellent materials in nature provides an alternative way to uncover the mechanisms of these materials. Lotus leaves, which remain clean despite growing in mud, are the most well known natural example of these

Received: December 6, 2015
Published: December 10, 2015

DOI: 10.1021/jacs.5b12728
J. Am. Chem. Soc. 2016, 138, 1727−1748

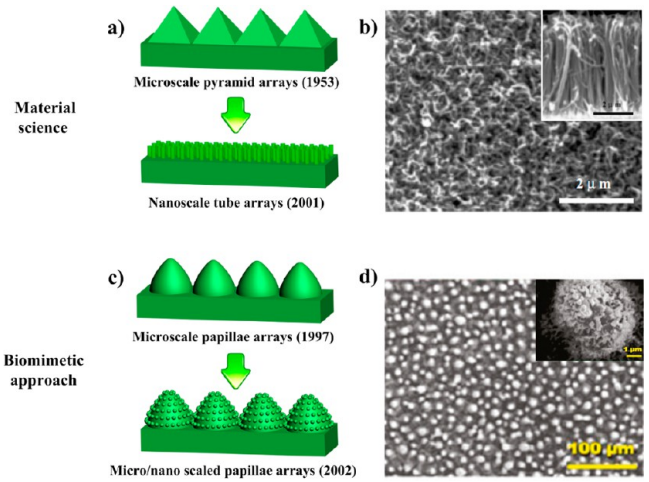

Figure 1. A detailed understanding of the role of nanoscale surface structures in building superhydrophobicity in air. (a) In the development of material design, sub-millimeter-scale pyramid-shaped paraffin surfaces were fabricated by Bartell and Shepard[7] in 1953 to exhibit an anti-wetting ability. Notably, discovered in 2001, individual nanoscale carbon nanotube arrays fabricated by Jiang et al.[8] could exhibit both superhydrophobic and superoleophobic properties. (b) SEM image of nanoscale vertical carbon nanotube arrays exhibiting both superhydrophobic and superoleophobic properties. Reproduced with permission from ref 8. Copyright 2001 Wiley. (c) From the biomimetic approach, Barthlott et al.[12] proposed an individual microstructured model to explain the mechanism of superhydrophobicity in 1997. However, the water droplets were easily pinned on the microstructured surfaces. In 2002, Jiang et al.[14] found that micro- and nanoscale two-tier structures were the key to superhydrophobicity, triggering the fabrication of superhydrophobic surfaces with low adhesion. (d) SEM image of lotus-inspired carbon nanotube patterns exhibiting ultra-high anti-wetting ability. Reproduced with permission from ref 14. Copyright 2002 Wiley.

materials. In 1997, Barthlott et al. posited that the microstructures of the lotus leaves were the key to the leaves' superhydrophobicity.[12] This hypothesis prompted researchers to build microstructure-based superhydrophobic materials that imitated natural phenomena (Figure 1c). However, water droplets easily adhered to the resulting microstructured surfaces.[13] In 2002, Jiang et al. reported that micro- and nanoscale two-tier structures were actually the key structural features of lotus leaves that allowed them to remain superhydrophobic in air (Figure 1d).[14] After the authors removed the nanostructures using a heat treatment while leaving the microscale parts intact, the water droplets adhered to the microstructure-only surface. In materials science strategies, the surface structures can also develop from the aforementioned microscale pyramid arrays to nanoscale tube arrays, which was reported by Jiang et al. in 2001 (Figure 1b).[8] A nanostructured material composed of aligned carbon nanotube films exhibited a superamphiphobic (i.e., both superhydrophobic and superoleophobic) property, indicating the importance of nanostructures in building anti-wetting surfaces. The importance of micro-/nanoscale two-tier structures in superhydrophobicity has also been demonstrated by Koch et al.[15] and Robin et al.[16] Microscale pillar arrays failed to transfer from the Wenzel state to the Cassie state by negative Laplace pressures, whereas micro-/nanoscale two-tier-structured surfaces succeeded in the reversible transition between these two states (Figure 2).

Another breakthrough in the field of materials science was the first discovery of superhydrophilicity in the development of silicon wafer pretreatment in 1959.[17] More specific research

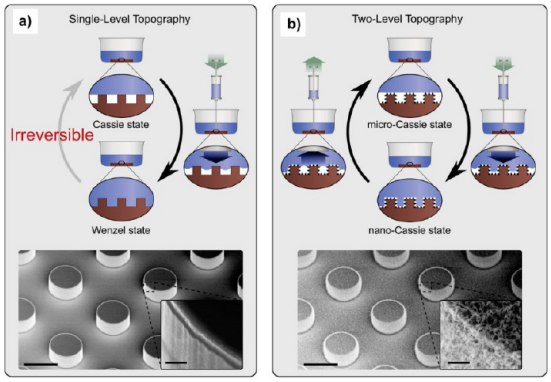

Figure 2. Micro-/nanoscale two-tier structures are the key factor in building stable superhydrophobic surfaces. Micro-/nanoscale two-tier structures can contribute to a nano-Cassie state under positive pressure. Thus, water was repelled when the external force was reduced. Differently, the individual microstructure only changed into a Wenzel state under positive pressure and could not be reversed. (a) For single microscale roughness, an irreversible change in the wetting behavior from the Cassie to the Wenzel state appeared. (b) For their hierarchical counterpart, nanostructures can replace the Wenzel state with a nano-Cassie state due to the trapped air pockets inside their structural gaps. Reproduced with permission from ref 16. Copyright 2012 National Academy of Sciences, USA.

demonstrated that the superhydrophilic surfaces comprised both hydrophilic hydroxy and hydrophobic epoxy at room temperature.[18] Fujishima et al. demonstrated another type of superhydrophilic surface based on the photoirradiation of TiO_2-coated glass slides.[19] These superhydrophilic materials have received more attention due to their various applications such as self-cleaning and anti-fogging. In 2009, research on wettability was extended to oil/water/solid phases, i.e., materials that are superamphiphilic in air but superoleophobic under water,[20] thus prompting a new wave of research in this field. From continuing studies on superwettability properties,[21−23] including superhydrophilicity, superoleophilicity, superhydrophobicity, and superoleophobicity in air; superoleophilicity, superoleophobicity, superaerophilicity, and superaerophobicity under water; and superhydrophilicity, superaerophilicity, superhydrophobicity, and superhydroaerophobicity under oil, a superwettability system was demonstrated in 2014[13] that attracted considerable attention from researchers in diverse backgrounds.

In addition to the increasing attempts to fabricate superwettable materials, recent research has focused on applications, especially in chemistry, for these unique interfacial materials. Because of their low-adhesion properties and/or the solid/liquid/gas three-phase contact model, chemical behavior on superwettable surfaces is quite different compared with that on traditional solid/liquid two-phase interfaces. In this Perspective, we will first introduce the evolution of the study of superwettable materials, mainly focusing on the fundamental rules for building these liquid-repellent materials. In the following sections, we will discuss recent applications of superwettable materials in altering the behaviors of chemical reactants and products. Some unique applications, such as superwettable-surface-based crystallization and microfabrication, will also be briefly summarized. Finally, we will discuss future developments in superwettable materials and their application in chemistry. We will mainly address the following two topics: how chemistry can facilitate the fabrication of superwettable materials, and what contributions these materials can provide to chemistry. We will attempt to

DOI: 10.1021/jacs.5b12728
J. Am. Chem. Soc. 2016, 138, 1727−1748

demonstrate the mutual benefits offered by superwettable materials and chemistry.

2. SUPERWETTABLE INTERFACIAL MATERIALS

2.1. Superwettability in Air. *2.1.1. Superhydrophobicity and Superoleophilicity.* Research on superhydrophobic materials can trace its history to 1907,[5,6] when Ollivier reported that virtually spherical droplets were present on surfaces consisting of soot, lycopodium powder, and arsenic trioxide. In 1923, Coghill and Anderson demonstrated that rough galena surfaces covered by stearic acids could exhibit a high water contact angle (CA, also represented as θ) of ca. 160°.[24] Consequently, Bartell and Shepard reported pyramid-shaped paraffin surface structures that effectively repelled water droplets.[7] In 1996, Onda et al. used a "bottom-up" strategy to introduce roughness onto alkyl ketene dimer films, thereby creating superhydrophobic surfaces with a CA of 174°.[9] Sporadic reports of the fabrication of superhydrophobic materials appeared during this period. Notably, the general/universal mechanism for building anti-wetting materials remains unclear.

In the biomimetic approach, the imitation of surfaces found in nature is an alternative way to design superhydrophobic materials. In 1997, Barthlott and Neinhuis discovered the self-cleaning properties of the lotus plant when investigating several types of plant leaves.[12] They attributed this low-adhesion superhydrophobic property to the microscale papillae incorporated into hydrophobic epicuticular wax. However, their single-microscale roughness model could not explain the low adhesion of lotus leaves, as noted by Jiang et al. in 2002.[14] In their study, branch-like nanostructures were observed upon the tops of the microscale papillae that created the micro- and nanoscale two-tier roughness responsible for the self-cleaning ability (Figure 3a). In a control experiment, by removing the nanostructures through a heat treatment while retaining the microstructures of lotus leaves, the authors found that water droplets could not roll on the microstructured surfaces. In addition to lotus leaves, the legs of water striders[25] (Figure 3b) and the eyes of mosquitos[26] (Figure 3c) are other examples of low-adhesion superhydrophobicity in organisms.

Nature also provides several examples of anisotropic superwettability. For example, water droplets easily roll along the direction parallel to the rice leaf edge rather than perpendicular.[14] This property was attributed to the anisotropic arrangement of microstructures on the leaves. The distribution of the papillae was in a quasi-one-dimensional order parallel to the leaf edge rather than a uniform arrangement like on the lotus leaf. In this case, water droplets would be induced to roll along the natural design. Similar to rice leaves, the butterfly wings (Figure 3d) also exhibit anisotropic rolling/pinning superhydrophobic states.[27] The water droplets on butterfly wings easily rolled away along the radial outward (RO) direction, but their movement was strongly inhibited in the opposite direction. An SEM investigation of the wings showed periodic hierarchical scales along the RO direction. Each scale was composed of well-oriented nanostripes, which were stacked stepwise by tilted periodic lamellae along the RO direction. Interestingly, the nanoscale tips on the top of stripes tilted slightly upward, allowing the water droplets to roll along them but pinning the droplets when rolling against the tips.

In addition to these low-adhesion superhydrophobic examples, some organisms also provide examples of high-adhesion superhydrophobic properties, such as gecko feet (Figure 3e).[28,29] The surface of gecko feet consists of well-aligned microhairs called setae (approximately 5 μm in diameter and 110 μm in length), which are split into hundreds of smaller nanoscale ends called spatulae. Due to the microstructures, the van der Waals forces generated between the gecko spatulae and water droplets are considerable. Liu et al. reported that the adhesive force between gecko feet and water droplets was in the range of 10−60 μN, depending on conformational changes in the surface setae proteins upon exposure to water.[30] This natural example continues to inspire researchers to fabricate multifunctional materials with rationally designed adhesion and self-cleaning properties.

Hydrophobic materials commonly occur on the surfaces of anti-wetting plants and animals.[14,25−30] For example, plant cuticles are generally covered by epicuticular wax or other substances mainly consisting of straight-chain aliphatic hydrocarbons with different substituted functional groups. These chemical shields can effectively decrease surface wetting and moisture loss. Alternatively, animal skin and fur are mainly composed of keratin proteins. These types of hydrophobic chemical structures can protect animals from water permeation into their bodies. Therefore, the first rule informed by natural examples of superhydrophobicity is that the chemical compositions of the material surfaces should be hydrophobic.

Next, the definition of hydrophobicity should be carefully clarified. It is generally accepted that solid surfaces with water CAs >90° are defined as hydrophobic according to Young's equation. However, using a surface force apparatus supported by ancillary techniques, Volger et al. demonstrated that a CA of 65° divides solid materials into hydrophobic and hydrophilic, rather than 90° as in the mathematical concept.[31] Long-range attractive forces could be detected when two planes exhibited a water CA >65°. In contrast, repulsive forces appeared between surfaces with θ < 65°. This result clearly demonstrates that the new division of hydrophilicity and hydrophobicity should be 65° rather than 90° when considering the chemical and structural states of water droplets. Similar to this research, Jiang et al. found that an angle of 62.7° could distinguish between hydrophilicity and hydrophobicity after investigating the apparent and intrinsic CA of many polymeric materials.[32]

In addition to chemical composition, the surface structure is also a key factor in surface wettability. Therefore, a general rule for building superhydrophobic materials is the introduction of sufficient surface roughness onto natural hydrophobic materials.[13] Two general rules can be summarized for constructing superhydrophobic materials: generating sufficient roughness on the material surfaces, and tailoring the chemical compositions of material surfaces to be hydrophobic with a water CA >65° (Figure 3i).

Notably, superhydrophobic surfaces exhibiting similar apparent CAs can exhibit completely different CA hysteresis.[33,34] To distinguish between diverse superhydrophobic states, five typical cases for anti-wetting surfaces have been defined (Figure 4):[35] totally wetting superhydrophobic surfaces in the Wenzel state, totally air-supporting superhydrophobic surfaces in the Cassie state, surfaces in the micro-/nanostructured two-tier "lotus" state, the metastable state between the Wenzel and Cassie states (including a "petal" state), and a partially wetting "fecko" state.

2.1.2. Superhydrophilicity and Superoleophilicity. Nature also provides several examples for studying superhydrophilicity. Nepenthes pitcher leaves with microtextured peristomes or rims exhibit a superwetting property, which allows a thin layer of sticky liquid to cover their entire surface (Figure 3f).[36] In this case, the liquid-infused surfaces become highly slippery, and insects can easily fall into their pitcher-shaped leaves. Some aquatic animals, such as sharks[37] (Figure 3g), exhibit a

DOI: 10.1021/jacs.5b12728
J. Am. Chem. Soc. 2016, 138, 1727−1748

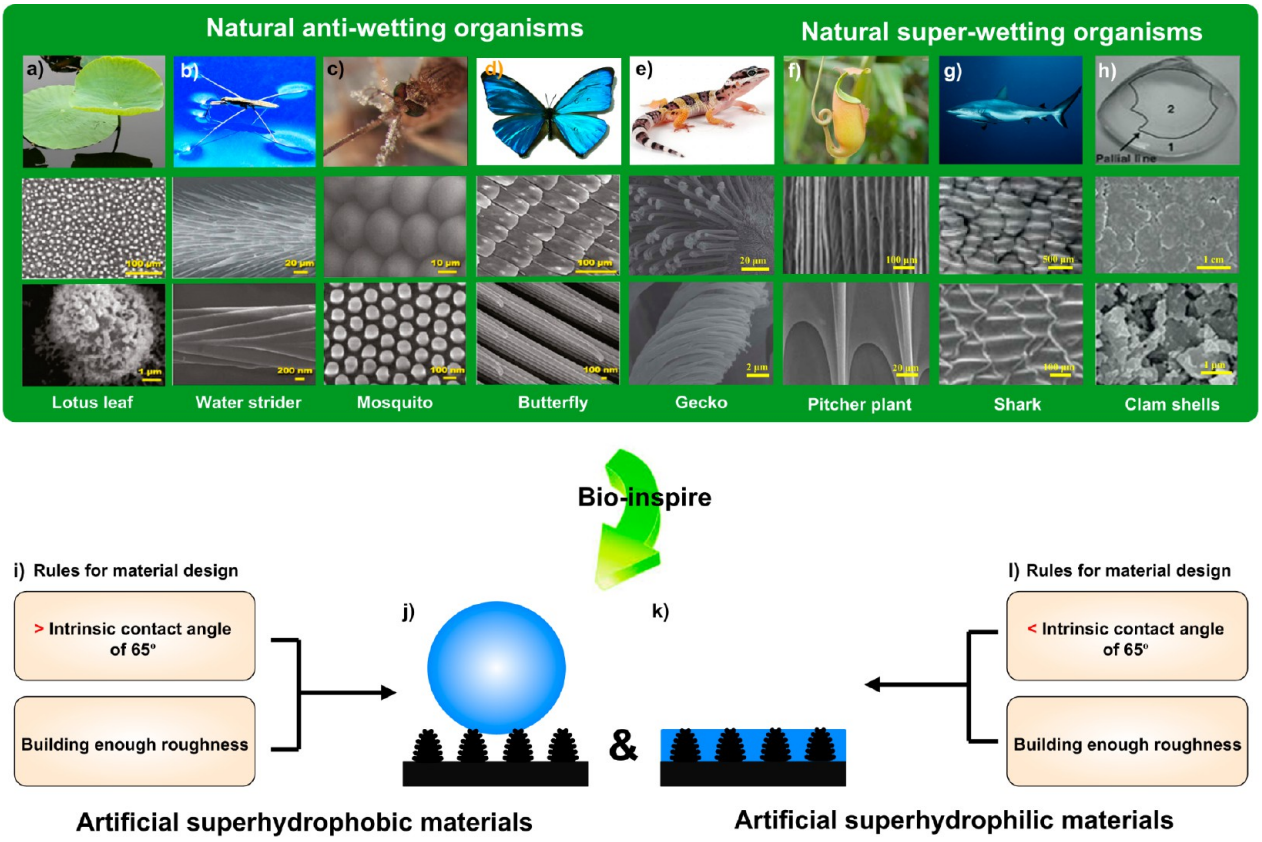

Figure 3. Natural organisms have inspired the design of superhydrophobic materials. Top section: (a) Lotus leaves demonstrate low adhesion, superhydrophobic, and self-cleaning properties, due to randomly distributed micro-papillae covered by branch-like nanostructures. Reproduced with permission from ref 14. Copyright 2002 Wiley. (b) Water strider legs have robust superhydrophobicity attributed to the directional arrangements of needlelike micro-setae with helical nano-grooves. Reproduced with permission from ref 25. Copyright 2004 Nature Publishing Group. (c) A mosquito's compound eyes have a superhydrophobic function due to micro-ommatidia covered by nano-nipples. Reproduced with permission from ref 26. Copyright 2007 Wiley. (d) Butterfly wings exhibit directional adhesion and superhydrophobicity due to the multiscale structures. Reproduced with permission from ref 27. Copyright 2007 The Royal Society of Chemistry. (e) A gecko's feet present highly adhesive superhydrophobic functions due to the aligned microsetae splitting into hundreds of nanospatulae. Reproduced with permission from ref 30. Copyright 2012 The Royal Society of Chemistry. (f) A pitcher plant that uses a superhydrophilic, highly slippery microstructured peristome or rim to capture insects. (g) A superhydrophilic shark skin consisting of hierarchical scales. Reproduced with permission from ref 37. Copyright 1999 Nature Publishing Group. (h) The superhydrophilic inner wall of clam shells. Reproduced with permission from ref 38. Copyright 2012 Wiley. Bottom section: The rules for building artificial (i) superhydrophobic and (l) superhydrophilic materials. The first rule states that the surfaces of materials should exhibit a $\theta >$ or $<65°$ water contact angle. The second rule is the introduction of sufficient roughness, such as two-tier micro-/nanostructures. In this case, (j) superhydrophobic or (k) superhydrophilic materials can be fabricated.

superwetting property on their skin that greatly reduces the drag force when they move under water. A similar superhydrophilic feature can also be found on the inner walls of clam shells[38] (Figure 3h). These examples represent two general types of features that contribute to superwetting, thin hydrogel-like layers and hierarchical surfaces.

Therefore, a general set of rules for fabricating superhydrophilic materials can be established. One rule is to generate sufficient roughness on the material surfaces, and the other is to tailor the chemical compositions of material surfaces to be hydrophilic with a water CA <65° (Figure 3l). For a deeper understanding of the development of superhydrophilic materials, many comprehensive reviews can be found in the literature.[39−41]

A special case for superhydrophilicity is intrinsic superhydrophilicity. Light irradiation, particularly with UV, can generate electrons and holes in semiconductors,[17,42] leading to an intrinsic superwetting phenomenon in silicon, even without microstructures. Fujishima et al. demonstrated a superhydrophilic surface via photoirradiation of TiO_2-coated glass slides.[19] Therefore, superhydrophilicity can be divided into structure-free intrinsic and structure-assisted categories (Figure 4). The latter category can be subdivided into three types of superhydrophobicity: individual microstructures, two-tier micro-/nanostructures, and porosity.

2.1.3. Superhydrophobicity and Superoleophobicity (Superamphiphobicity or Superomniphobicity). Generally, the surfaces of natural organisms are superhydrophobic yet oleophilic since water, rather than oils, is more abundant in their natural habitats. Because the surface tension of oils (~20−60 $mN{\cdot}m^{-1}$) is smaller than that of water (~72 $mN{\cdot}m^{-1}$), superhydrophobic materials in air are usually wetted by oils. However, with the rapid pace of anti-wetting research, materials that simultaneously exhibit superhydrophobic and superoleophobic properties have been fabricated. In 1997, Tsujii et al. reported an oil-repellent anodically oxidized aluminum plate modified by fluorinated monoalkylphosphate.[43] The high fractal dimension of the aluminum surface and the compact packing of the trifluoromethyl groups were two key factors in determining the low-adhesion oil-repellent properties. Subsequently, a series

DOI: 10.1021/jacs.5b12728
J. Am. Chem. Soc. 2016, 138, 1727−1748

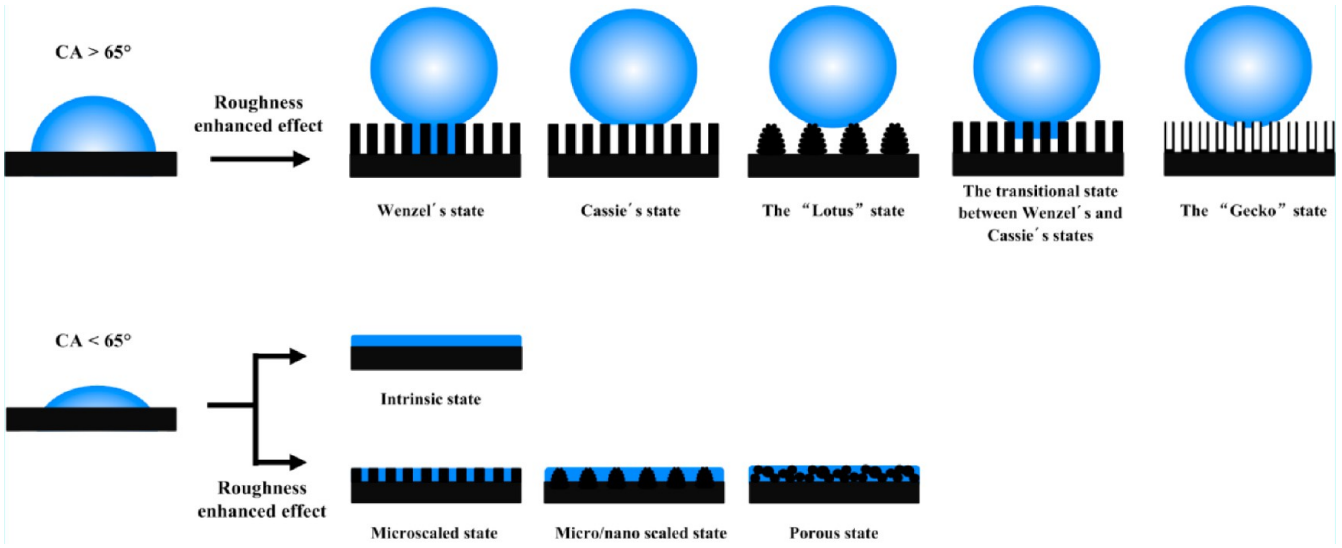

Figure 4. Definition of diverse superhydrophobic/superhydrophilic states. Top row: anti-wetting surfaces can exhibit fully wetting superhydrophobic surfaces in the Wenzel state, fully air-supporting superhydrophobic surfaces in the Cassie state, the micro-/nanostructured two-tier "lotus" state, the metastable state between the Wenzel and Cassie states (including a "petal" state), and a partially wetting "gecko" state. Bottom row: superwetting surfaces can be divided into intrinsic superhydrophilicity, i.e., without the assistance of microstructures or microstructured, two-tier micro-/nanoscale, and porosity-type superhydrophilic surfaces.

of studies on fabricating superoleophobic materials were carried out.[44,45]

In most cases, the intermolecular forces between oil molecules and solid surface molecules/atoms are attractive forces, which allow the oil to wet the surface. By modifying straight- or branched-chain molecules with fluoridated groups oriented outward on the surfaces, the intermolecular attraction between the oil molecules and solid surface can become repulsive. For example, Jiang et al. reported that aligned carbon nanotube films exhibited a water CA of 158.5 ± 1.5°, whereas rapeseed oil had a CA of 0° (i.e., complete wetting).[8] When covered by a layer of fluoroalkylsilane molecules, the intermolecular force between the oil molecules and solid carbon surface changed, producing a rapeseed oil CA of 161 ± 1°. This study demonstrates a convincing example that superoleophobicity can be generated by modifying the surface chemical composition without changing the surface microstructure.

Microstructures, such as hoodoo-like[46] or re-entrant structures,[47,48] can also be introduced to improve the oil repellency. Overhanging structures (Figure 5) can prevent oils from permeating the surface due to a considerable amount of trapped air pockets in the bottom gaps of the microstructures. Therefore, the oil makes contact with a composite air and solid surface, which exhibits apparent superoleophobicity. Re-entrant structures consisting of semicircular ridges and grooves are another interesting structural design for preventing the permeation of oil.[47,48] Because of the regular convex-concave microstructures, the oil could be pinned at a certain height on the microstructure, yielding a large static CA and a small sliding angle. Recently, high-fractal-dimension and fabric-based hierarchical microstructures have also been employed to prevent the wetting of oils.[49] By creating sufficient roughness combined with the construction of low-surface-energy fluoridated layers, diverse organic liquids from glycerol (surface tension of ~60 $mN \cdot m^{-1}$) to ethanol (surface tension of ~20 $mN \cdot m^{-1}$) could be repelled with low adhesion.

2.1.4. Superhydrophilicity and Superoleophobicity. It is commonly believed that superoleophobic surfaces are also superhydrophobic because the surface tension of oil (~20–60 $mN \cdot m^{-1}$) is smaller than that of water (~72 $mN \cdot m^{-1}$). Interestingly, Zhao et al. reported an unexpected surface exhibiting simultaneous superoleophobicity and superhydrophilicity.[50] A mixture of heptadecafluorononanoic-acid-modified TiO_2 sol (HFA–TiO_2) and silica nanoparticles was coated onto a sheet of polyester fabric. After the solvent evaporated, the rough surfaces exhibited superamphiphobicity with both water and oil CAs >150°. However, the wettability of the surface changed upon exposure to ammonia vapor for 30 s. The water CA decreased to 0°, while the oil CA remained approximately 150°. A possible explanation for this unusual phenomenon is the presence of titanium carboxylate coordination bonding on the HFA–TiO_2 coating after exposure to the ammonia vapor. In this case, the intermolecular force between the solid surface and the water droplet changed, while that between the solid surface and the oil remained the same, which yielded a superhydrophilic and superoleophobic material. A similar phenomenon has also been reported by Tuteja et al.[51]

2.1.5. Superlyophobicity or Superlyophilicity. The design of surface roughness can either trap or repel considerable amounts of air pockets inside gaps in the microstructure, creating either superlyophobic or superlyophilic materials that can either repel or attract, respectively, diverse types of liquids (Figure 6). The liquids can be single-component species, such as ionic liquids, metallic liquids, liquid crystals, and organic solvents. At the same time, the liquids can be multi-component hybrid liquids, e.g., acidic, alkaline, or saline aqueous solutions; polymeric liquids; biofluids including blood, saliva, or other tissue fluids; colloids; emulsions consisting of oil-in-water, water-in-oil, water-in-oil-in-water, or oil-in-water-in-oil types; magnetic or ferroelectric fluids; and other liquids in addition to water and oils.

Furthermore, the wettabilities of the surfaces can be extended to a wide range of pressures (from 1 atm to thousands of atm) or temperatures (from 1 to 3000 K) and can respond to diverse external stimuli, such as thermal or electrical stimuli, light, pH, ions, or molecules. This broad range of interactions will attract the attention of researchers in diverse fields because the

DOI: 10.1021/jacs.5b12728
J. Am. Chem. Soc. 2016, 138, 1727–1748

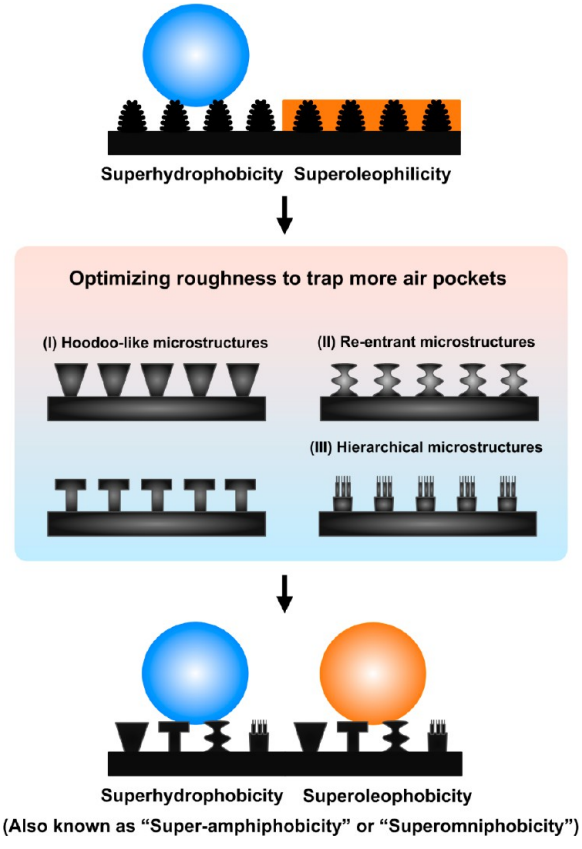

Figure 5. Reducing the surface energy and increasing the surface roughness are two key strategies to generate superamphiphobic, also known as superomniphobic, materials (i.e., simultaneously superhydrophobic and superoleophobic materials). Modifying the surface with low surface-energy molecules. Introducing hoodoo-like, re-entrant or hierarchical microstructures to trap more air pockets and to pin the liquid/solid contact lines to prevent the permeation of oil.

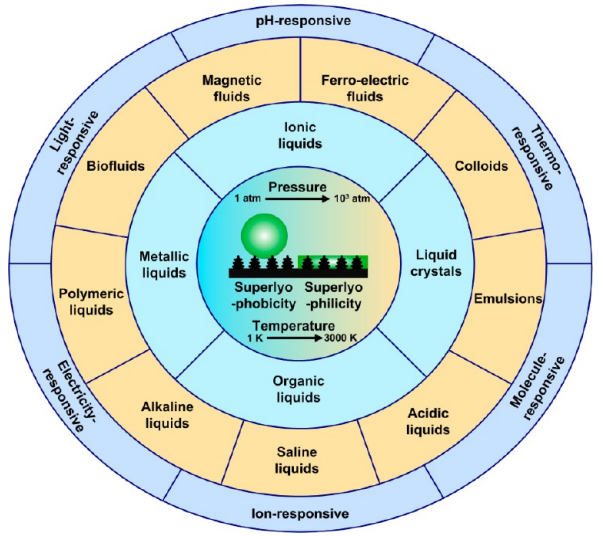

Figure 6. Building superlyophobic/superlyophilic materials through the novel design of surface chemical compositions and hierarchical microstructures. By generating repulsive/attractive forces among the solid/liquid interfaces and building considerable roughness, the as-prepared materials can repel/attract diverse liquids. The liquids can be single-component species, such as ionic liquids, metallic liquids, liquid crystals, and organic solvents. At the same time, the liquids will be multicomponent hybrid liquids, e.g., acidic, alkaline, or saline aqueous solutions; polymeric liquids; biofluids including blood, saliva, or other tissue fluids; colloids; emulsions consisting of oil-in-water, water-in-oil, water-in-oil-in-water, and oil-in-water-in-oil types; magnetic or ferro-electric fluids; and other liquids in addition to water and oils. The wettabilities of the surfaces can withstand different pressures (from 1 atm to thousands of atm) and temperatures (from 1 to 3000 K) and respond to diverse external stimuli, such as temperature, electricity, light, pH, ions, or targeted molecules.

solid/liquid interface is a common issue in many fields. The careful selection of surface chemical compositions and the novel design of hierarchical microstructures can possibly enhance the performance of liquid-repelling/attracting materials.

2.2. Superwettability in Other Media. *2.2.1. Superaerophobicity and Superaerophilicity under Water.* In nature, many organisms live in or around water. To breathe under water without gills, water spiders, also called diving bell spiders, employ an alternative breathing system by building a physical external lung consisting of large air bubbles on their abdomen and legs.[52] Thanks to their hydrophobic skin with rough fiber-like structures, to which bubbles anchor firmly, yielding underwater superaerophilicity. These bubbles allow them to conduct their daily lives, including preying on food. Plants, such as lotus leaves, can also exhibit underwater superaerophobicity. Air bubbles quickly burst on these underwater superaerophobic surfaces when they are faced downward toward water (Figure 7a).[53]

Inspired by these natural organisms, researchers have fabricated artificial underwater superaerophilic/superaerophobic materials using vertically aligned silicon nanowires (Figure 7c).[53] A bubble CA of 157.8 ± 8.5° appeared on these surfaces when immersed in water. By tailoring of the pillar gaps and sizes, the rough surfaces can be made to exhibit underwater superaerophilicity with a bubble CA of 0° within only 0.2 s. Jiang and Su et al. reported that, due to this excellent bubble-absorbing ability, underwater superaerophilic sponges could be used to selectively absorb methane bubbles in water.[54] Significantly, the collected bubbles were able to be transported by a pipe in contact with the sponge, regardless of where they were absorbed. This simple yet effective technique provides a promising way to harness marine methane emissions to potentially alleviate global warming. Recently, underwater superaerophobic porous copper wires have been reported to efficiently capture and directionally transport gas bubbles in water.[55]

When a solid surface is immersed in an aqueous environment, it first comes into contact with water, rather than air. Thus, the third phase, i.e., gas bubbles, competes with the water to approach the surface. Depending on the chemical compositions of the surfaces, the intermolecular forces between the solid and water and those between the solid and gas determine the wetting state on the substrate. To build underwater superaerophobic materials, attractive forces are necessary between the solid surface and water, and repulsive forces are necessary between the solid surface and the gas. Together with considerable surface roughness, these surfaces could exhibit an underwater gas-repellent property. In other words, the chemical composition on the rough surfaces determines the wetting state in diverse environments. Superhydrophilic materials in air would be superaerophobic under water, whereas superhydrophobic materials in air would be superaerophilic under water.

2.2.2. Superoleophobicity and Superoleophilicity under Water. Oil leakage into terrestrial bodies of water can be an environmental disaster. For example, seabirds can die because of oil wetting the feathers on their wings. In contrast, most types of

DOI: 10.1021/jacs.5b12728
J. Am. Chem. Soc. 2016, 138, 1727−1748

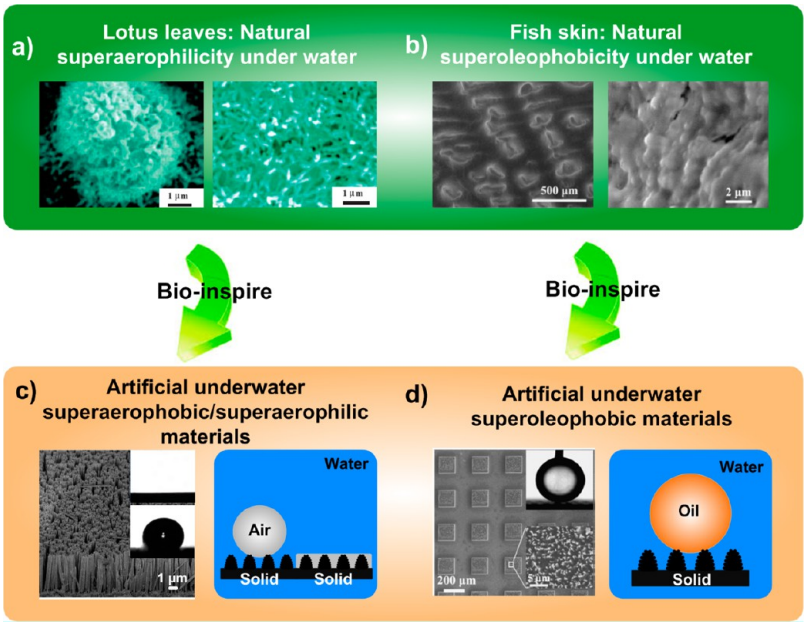

Figure 7. Natural organisms inspire the design of underwater superaerophobic/superaerophilic/superoleophobic materials. (a) SEM images of lotus leaves. Reproduced with permission from ref 14. Copyright 2002 Wiley. (b) SEM images of fish skin. Reproduced with permission from ref 20. Copyright 2009 Wiley. (c) Artificial underwater superaerophobic/superaerophilic materials. Left: SEM image of surfaces with aligned silicon nanowires, which exhibit underwater superaerophobicity/superaerophilicity. Reproduced with permission from ref 53. Copyright 2009 American Chemical Society. Right: schematic illustration of underwater superaerophobic/superaerophilic surfaces. The solid surface repels/attracts the air molecules, mostly oxygen and nitrogen, while attracting/repelling water molecules. (d) Artificial underwater superoleophobic materials. Left: SEM image of surfaces with aligned silicon pillars, which exhibit underwater superoleophobicity. Reproduced with permission from ref 20. Copyright 2009 Wiley. Right: schematic illustration of the underwater superoleophobic surfaces. The solid surface repels oil molecules while attracting water molecules.

fish can keep their bodies clean. This interesting phenomenon inspired us to study the underwater superoleophobicity in nature.[20] Generally, rough fish scales are covered by a layer of mucus mainly consisting of a hydrogel. Due to this hydrophilic chemical composition on the surfaces and hierarchical scale structures, fish skin exhibits superhydrophilicity in air and superoleophobicity under water with an oil CA of 156.4 ± 3.0°. Short clams, another type of underwater superoleophobic organism, always remain clean on the outside and internal surfaces of their shells, especially on the pallium-covered region.[38] The inorganic $CaCO_3$ composition of their shells and their surface hierarchical structures are two key factors in determining their underwater oil repellency.

Learning from natural organisms, scientists have fabricated artificial underwater superoleophobic materials using pillar-arrayed silicon substrates (Figure 7d).[20] To increase the roughness, vertically aligned nanowires were generated on the micropillars. As a result, an oil droplet CA of 174.8 ± 2.3° appeared on these surfaces when they were immersed in water. In contrast, smooth and micropillar-structured silicon substrates exhibited oil droplet CAs of 134.8 ± 1.6° and 151.5 ± 1.8°, respectively. Although underwater superoleophobicity could be generated by etching silicon substrates, these substrates were easy to break and not very robust. Considering the complex hydrodynamic factors in underwater environments, building tough underwater oil-repellent materials is very challenging. Jiang et al. reported a robust underwater superoleophobic material fabricated by hierarchical macromolecule-nanoclay hydrogels.[56] Because of the nanoclays, the materials could withstand almost 2.5 MPa at 75% strain. These novel materials were coated on a copper mesh and, because of their superhydrophilicity in air and superoleophobicity in water, were able to selectively separate water from water/oil mixtures, including gasoline, diesel, vegetable oil, and even crude oil/water composites.[57] Because the adhesion between the oil droplets and the surface was considerably low, the underwater oil-repellent surfaces were able to control the movement of oil droplets in water.[58]

Similar to underwater superaerophobicity, water, rather than air, makes first contact with underwater superoleophobic solid surfaces. In this case, the third phase, i.e., the oil droplets, competes with the water to approach the surfaces. Controlling the chemical compositions of the surfaces determines the intermolecular forces between the solid and water and those between the solid and oils. To build underwater superoleophobic materials, attractive forces should occur between the solid surface atoms/molecules and water molecules, while repulsive forces should appear between the solid surface and the oil molecules. After sufficient roughness is induced, these surfaces can exhibit underwater oil repellency. In summary, materials that are superhydrophilic in air will also attract water molecules in an aqueous environment, yielding superoleophobic surfaces under water when in contact with oil droplets.

2.2.3. Superhydrophobicity and Superhydrophilicity under Oil. Most oils are immiscible with water. Once the gaps in rough surfaces are filled with pockets of oil rather than air, the as-prepared surfaces can exhibit water repellency. To demonstrate this concept, Jiang et al. generated solvent-evaporation-determined rough surfaces consisting of a mixture of nanoparticles and polymers.[59] Due to the oleophilicity of these surfaces, silicone oil could easily wet and then permeate into the gaps in the surfaces. The oil pockets were able to prevent the solid from contacting the water droplets. Thus, the surfaces exhibited water repellency with a water CA of 176.5 ± 3.3° when immersed in silicone oil. In this case, the intermolecular forces between the solid surface atoms/molecules and the oil molecules overcame the forces between the surface atoms/molecules and

DOI: 10.1021/jacs.5b12728
J. Am. Chem. Soc. 2016, 138, 1727−1748

the water molecules. Together with considerable roughness, these surfaces could exhibit under-oil water repellency. Furthermore, the authors evaluated smooth, microrough, nano-rough, and micro-/nano-rough silicon substrates modified by a fluoride compound by immersing the substrates in oil. The authors found that the smooth sample exhibited superhydrophobicity and aerophobicity, whereas the other three types of samples exhibited unexpected superhydrophobicity and superaerophobicity.[60] A possible explanation is that the intermolecular forces between the solid atoms/molecules and the oil molecules were considerably stronger than those between the solid and water or air.

2.3. A System of Superwettability. From the above introduction of the extreme wetting states, a clearly evolving understanding of the interaction between liquids and solids in diverse environments can be observed. The surface chemical composition determines the intermolecular forces at the interfaces between the solid, the liquid/air, and the environmental phase, while surface roughness optimizes/enhances these types of intermolecular forces. Thus far, interfacial materials designed with diverse superwetting states[13] consisting of superhydrophobicity, superhydrophilicity, superoleophobicity, and superoleophilicity in air (see the middle section of Figure 8); superoleophobicity, superoleophilicity, superaerophobicity, and superaerophilicity under water (see the left section of Figure 8); and superhydrophobicity, superhydrophilicity, superoleophobicity, and superoleophilicity under oil (see the right section of Figure 8) have been summarized. These diverse types of superwetting states serve as important building blocks in constructing a "superwettability" system.

2.4. Outlook: Superwettability in Other Media. From the above discussion, we can conclude that the chemical composition of solid surfaces is very important in controlling the intermolecular forces between the solid, liquid/gas and environmental phase. Diverse liquids, such as ionic liquids, metallic liquids, liquid crystals, organic liquids, and multi-component hybrid liquids (e.g., acidic, alkaline, or saline aqueous solutions; polymeric liquids; biofluids; colloids; emulsions; magnetic fluids or ferroelectric fluids; and others in addition to water and oils), can be considered as the objects of repulsion or attraction (Figure 9). Furthermore, the environmental phase can also be replaced by the above-mentioned liquids or different gas compositions. After sufficient roughness is induced onto solid surfaces, these functional liquids can be trapped in the surface gaps to prevent the permeation of other liquids, or they can be totally repelled by other liquids trapped in the gaps. Therefore, unforeseen systems of superwettability can be extended from the existing research (Figure 8).

3. SUPERWETTABILITY-BASED CHEMISTRY AND MICROFABRICATION

A third phase of matter exists at the interface between the gas or liquid and the surfaces of superwettable materials. In this case, chemical reactions and microfabrications may exhibit unexpected behavior compared with those on traditional two-phase surfaces. Thus, the effective collection of reaction products, unique growth models of precipitates, and a simple strategy for the alignment/assembly of nanoscale building blocks are potential applications for superwettable materials. Having discussed the evolution of superwettability, we will now address how these superwettable materials can make a contribution to chemistry. We will attempt to demonstrate the mutual benefits of superwettable materials and the field of chemistry (Figure 10).

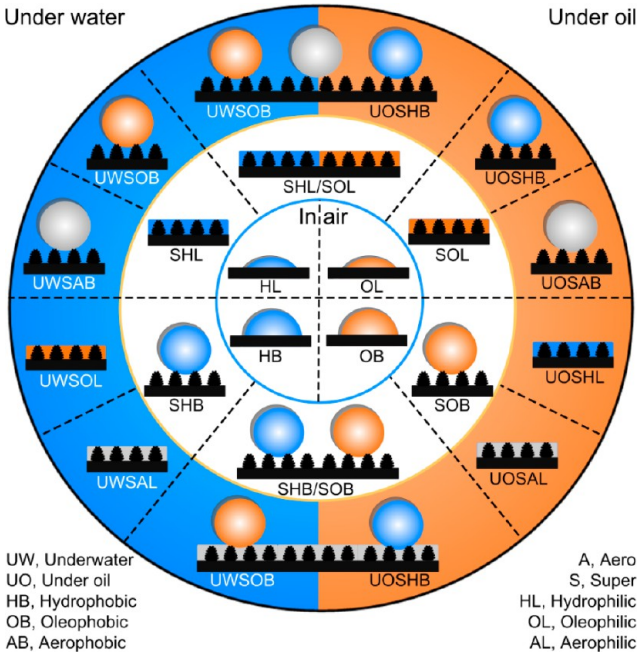

Figure 8. The system of "superwettability". Middle: hydrophilicity, oleophilicity, hydrophobicity and oleophobicity on smooth surfaces in air. After sufficient micro-/nanoscale hierarchical roughness is induced, the superhydrophilicity, superoleophilicity, superhydrophobicity and superoleophobicity states can be obtained in air. Left blue circle: underwater superoleophobicity, superoleophilicity, superaerophobicity and superaerophilicity on rough substrates; right orange circle: under-oil superhydrophobicity, superhydrophilicity, superoleophobicity and superoleophilicity on rough substrates. Diverse types of extreme wettability have served as important building blocks to construct a "superwettability" system. Reproduced with permission from ref 13. Copyright 2014 Wiley.

3.1. Unique Chemical Reactions on Superwettable Interfaces. As discussed in section 2.1.1, the air pockets inside the structural gaps of superhydrophobic materials can repel water droplets and generate ultra-low adhesion. By exploiting this advance in superhydrophobic materials, at least three types of strategies can be used to favor chemical reactions (Figure 11, left section). Due to the low adhesion property, the reaction reagents/products can be effectively used. The upward solid/liquid/gas three-phase contact line can restrict the formation/aggregation of products. Furthermore, if the interconnected surface gaps are filled with air and in contact with the ambient atmosphere, the surface gaps are able to continuously transport gaseous reactants into the liquid reactors. Alternatively, the superhydrophilic surfaces can be used as ultra-slippery interfaces due to the fully wetted oil layers in the structural gaps (Figure 11, right section). Moreover, two layers of immiscible liquids can wet the superhydrophilic surfaces in a stepwise manner, yielding an ultra-thin layer of products between these two reactant liquid films. An ultra-thin film can be generated from the rapid and complete permeation of the liquid into this type of surface.

3.1.1. Ultra-low Adhesion of Superhydrophobic Surfaces. Adhesion often occurs between the chemical reactants and/or products and the reaction vessels.[61] This adhesion can waste many valuable reagents/chemicals and block thermal/mass transport due to the considerable amount of residue. Exploiting the low adhesion of superwettable materials is a promising way to address this issue. When chemical reactions are performed on these unique interfaces, the reactants and/or products dissolved

DOI: 10.1021/jacs.5b12728
J. Am. Chem. Soc. 2016, 138, 1727−1748

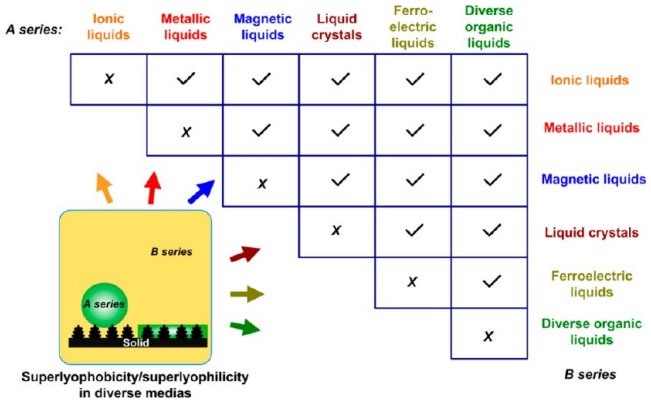

Figure 9. By replacing the target repellent materials or environmental phase by diverse liquids, such as ionic liquids, metallic liquids, liquid crystals, organic liquids and multi-component hybrid liquids (e.g., acidic, alkaline or saline aqueous solutions; polymeric liquids; biofluids; colloids; emulsions; magnetic fluids or ferroelectric fluids; or others in addition to water and oils), the superwettability system can be enriched from existing states to future unexpected states. The "×" represents the same material existing in the target matter and environmental phase. Thus, no superlyophobic/superlyophilic states occur in these cases. The "√" represents the possibility of superlyophobic/superlyophilic states in the target matter and environmental phase. For example, rough surfaces might exhibit a highly ionic-liquid-repellent property when they are immersed in the metallic liquid.

in the liquid droplets will be repelled, thereby improving the effective yield of the obtained products.

a. General Reactions. Generally, the precipitation reaction leaves a residue of reaction products on the bottom of the reactors. To fully harvest the products and clean the reactor, superhydrophobic tweezers and related tools with low adhesion have been used to manipulate droplet motion on demand and perform a "clean" precipitation reaction (Figure 12b).[62] The anti-wetting coatings on the tweezers and substrates consisted of polymer/hydrophobic nanoparticles. Due to the evaporation of organic solvent, both surface microstructures and low surface energies could be generated on the coatings, allowing these coated tools to manipulate the droplets with no adhesion. As a result, a droplet could be picked up directly and released precisely by carefully opening the tweezer tips. Then, the two droplets containing different reagents could coalesce to yield a droplet-based chemical reaction. After the complete reaction of these two reagents, the precipitation products were completely collected by the unique low adhesion of the polymer/nanoparticle composite coatings. Significantly, this superwettability-based reaction system exhibited two advantages: the effective use of reactants and the complete collection of products.

In addition to superhydrophobic surfaces in air, underwater superoleophobic materials have been used to perform oil-droplet-based chemical reactions.[58] Rough glass plates were fabricated as the tweezers and the base. Then, a tetrachloromethane droplet containing 5% (v/v) bromine was manipulated to coalesce with another droplet containing 5% styrene (Figure 12c). After approximately 1 min, the coalesced droplet became transparent, indicating that an addition reaction had occurred inside the droplet-based reactor. Furthermore, by immersing an aqueous droplet containing calcium acetate and urea in 80 °C silicone oil for 24 h, urchin-shaped $CaCO_3$ microspheres were generated.[63] Due to the ultra-low adhesion of the surfaces in the oil (4.4 ± 0.7 μN for a 20 μL water droplet), the white precipitates could be completely collected from the oil

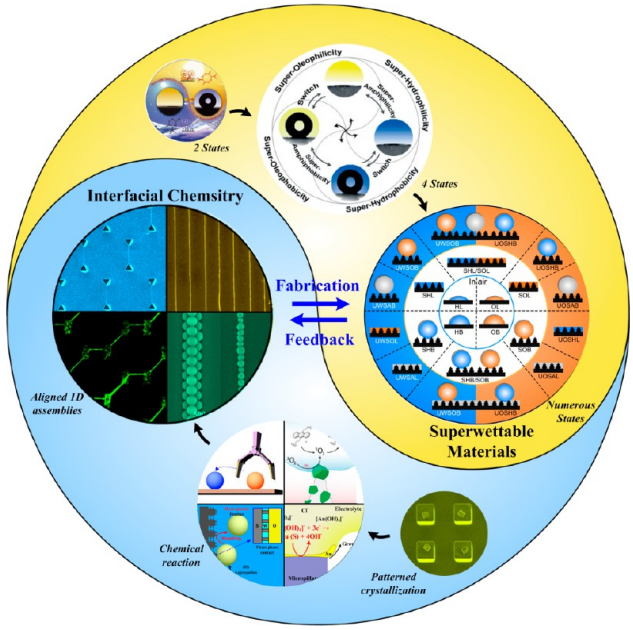

Figure 10. Mutual promotion of superwettable materials and chemistry. The scope of this Perspective involves a discussion of using chemistry to fabricate the superwettable materials and the way that these unique materials affect the behaviors of chemistry and microfabrication. In the beginning, opposite superhydrophobicity/superhydrophilicity states were recognized, followed by the extension to four states: superhydrophobicity, superhydrophilicity, superoleophobicity, and superoleophilicity. In 2014, the system of "superwettability" was proposed by Jiang et al.[12] after exploiting numerous states of extreme wettabilities. Understanding the superwettable system inspired research on the chemistry/microfabrication on superwettable surfaces. Using the low adhesion of superhydrophobic surfaces, microscale crystal arrays with on-demand positions can be fabricated. Meanwhile, the reactants and products can be effectively used and collected when the chemical reactions occur on the anti-wetting surfaces. Furthermore, this low adhesion facilitates the yield of gas generation reactions and other electrical reactions. The gas pockets trapped in the structural gaps of anti-wetting surfaces can be used as channels to continuously transport the gas reaction from the environment to the liquid. Notably, the solid/liquid/gas three-phase contact line can also be used to restrict the growth of the reaction products, allowing overhanging microstructures that cannot be formed on normal surfaces. The airpockets inside superhydrophobic surfaces can guide controllable rupture of liquid films, yielding diverse building blocks, including macromolecules, small molecules, and nanoparticles, into regular 1D patterns. Adapted with permission from refs 12, 94, 101, 102, and 103. Copyright 2012−2014 Wiley.

(Figure 12d). This residue-free chemical reaction system may have promising applications in the small-scale fabrication of biological medicines and toxic chemicals. Lin et al. reported an alternative way to use hydrophobic Fe_3O_4 powders to build marble-based microreactors.[64] Two types of chemiluminescence reactions were performed inside the marbles. Importantly, changing the amount of reaction liquid inside the marble reactors was easy due to the low adhesion between the hydrophobic powders and the water.

b. Polymerization Reactions. Due to the low adhesion of superamphiphobic surfaces, organic liquids, such as styrene or methacrylate, can be polymerized to form microspheres without a solvent. Vollmer, Butt, et al. generated superamphiphobic surfaces enhanced by rough fractal-like soot microstructures (Figure 13a).[65] To increase their transparency, a 20−30 nm thick

DOI: 10.1021/jacs.5b12728
J. Am. Chem. Soc. 2016, 138, 1727−1748

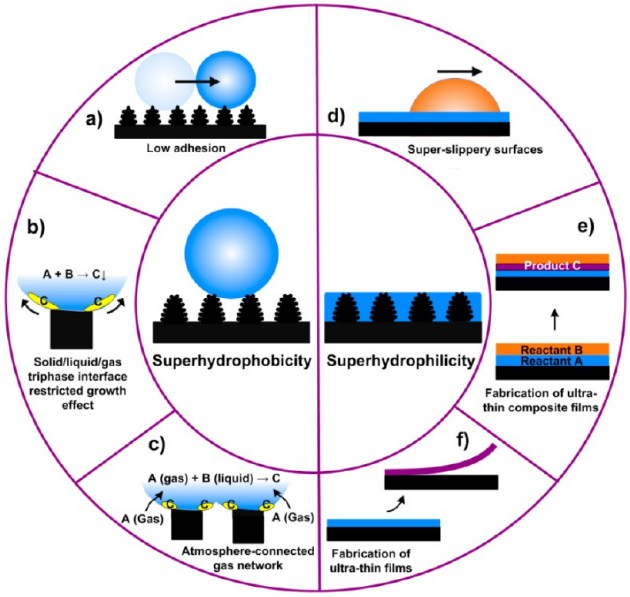

Figure 11. Proposed strategies for superwettable materials-based chemistry. For superhydrophobic surfaces: (a) due to the low adhesion of the superwettable surfaces, reaction products can be effectively collected when performing chemical reactions on these interfaces; (b) the curved solid/liquid/air three-phase contact line on the superwettable surfaces can restrict the growth of products; (c) due to the atmospherically connected gas network in the structural gaps on the superhydrophobic/superoleophobic surfaces, gas-phase reactions can occur along the curved solid/liquid/air three-phase contact line on the superwettable materials. For superhydrophilic surfaces: (d) a thin layer of low-surface-energy oil can fully wet the surface, yielding solid/liquid/liquid-type superslippery interfaces; (e) two layers of immiscible liquids can wet the superhydrophilic surfaces in a stepwise manner to yield an ultra-thin layer of products between these two reactant liquid films; (f) due to the rapid and complete permeation of the liquid onto this type of surface, an ultra-thin solid film can be generated after the evaporation of solvent.

layer of silica was coated and then modified by low-surface-energy fluoride compounds. As a result, on these superamphiphobic surfaces, even nonpolar liquids exhibited an apparent CA above 150° and a sliding angle below 10° in air. Then, the styrene bisphenol A glycerolate dimethacrylate, tri(ethylene glycol) dimethacrylate, and the photoinitiator phenylbis(2,4,6-trimethylbenzoyl) phosphine oxide were dropped onto the liquid-repellent surfaces, resulting in radical polymerization upon exposure to UV irradiation. After several minutes of polymerization, size-controlled microspheres were fabricated without the participation of a solvent. Because the superamphiphobic layers were stable up to 400 °C, a thermoplastic polymer powder, e.g., polystyrene, was able to form microspheres on these surfaces when heated above its glass transition temperature. Following this concept, a Janus microsphere consisting of half polystyrene and half poly(methyl methacrylate) was successfully fabricated by melting the polymeric powders under different temperatures. Recently, that same group of researchers used the same strategy to fabricate mesoporous TiO_2 superparticles.[66]

c. Electrochemical Reactions. Kolbe electrolysis is one of the most important applications of electrochemistry due to its high product selectivity and convenient manipulation.[67,68] In a typical Kolbe electrolysis reaction, hydrophilic carboxylic acids are decarboxylated under the influence of an electric field and converted into hydrophobic oil-like alkyl compounds. In general, flat platinum plates are used as the electrodes. However, reaction products easily adhere to the electrode surfaces due to their oleophilic character. As a result, the effective electron transfer area on the electrodes can be gradually reduced, which leads to an unstable current density in the electrolyte and even the termination of the electrochemical reaction. Thus, maintaining good contact with the hydrophilic reactants while simultaneously repelling the hydrophobic products is a significant challenge in Kolbe electrolysis. Using underwater superoleophobic platinum electrodes is proposed for Kolbe electrolysis (Figure 13b). Due to dual-scale micro-/nanostructures on the platinum plates, hydrophilic reactants would make close contact with the electrodes, allowing continuous electron transfer from the electrode to the electrolyte. Meanwhile, hydrophobic alkyl products would be repelled due to the water pockets trapped inside the microstructured gaps. As a result, this underwater superoleophobic electrode could at least double the working life of Kolbe electrolysis compared with the traditional oleophilic flat electrodes. A promising application of this type of long-lived Kolbe electrolysis is treating the surfactant-rich wastewater produced by human and industrial activities.

Direct liquid-feed fuel cells that oxidize liquid fuels (such as hydrazine and methanol) into gas products (N_2 and CO_2) have attracted tremendous amounts of attention in recent years. The release of gas products from the electrode surface should be fast and complete. Otherwise, the residual gas may block the transport of liquid fuels and provide a higher pressure in the flow field, thus deteriorating the fuel crossover. To address this challenge, Sun et al. recently used underwater superaerophobic copper films as the electrodes.[69] Vertically aligned nanoplates were formed on the copper films through an electrodeposition process. This porous structure and its hydrophilic character minimized the copper electrodes' adhesion to the gas bubbles. As a result, the release speed of the obtained nitrogen bubbles was faster than on the planar electrode with no nanostructures. Consequently, the Cu-nanostructured film exhibited high current densities, small overpotentials and long-term stability. When these cu films were used as the electrode in actual direct hydrazine fuel cells, the peak power density of the cells increased ~3 times compared with those using a commercial Pt/C anode, thus indicating that the high-efficiency fuel cells were improved by the superwettable materials.

The rapid release of bubbles from the electrodes can also favor the electrocatalytic hydrogen evolution reaction. By using underwater superaerophobic nanoarrayed platinum electrodes, Sun et al. found that the current density of the reaction was 13.75 times higher than that on the flat platinum counterpart (Figure 13c).[70,71] A similar concept has also been reported by Jin et al.[72] In their study, three types of metallic cobalt pyrite films—flat, microwire, and nanowire structures—were used as the electrode in the electrocatalytic hydrogen evolution reaction (Figure 13d). The increased underwater gas-repellent ability caused by the microstructures prompted the release of gas bubbles from the electrode surface. The CoS_2 nanowire electrodes could achieve geometric current densities of -10 mA cm^{-2} at overpotentials as low as -145 mV, thus exhibiting an improved electrocatalytic ability caused by the underwater aerophobic materials.

3.1.2. Interfacial Reactions Mediated by the Three-Phase Contact Line. In traditional solid/liquid two-phase reaction systems, the products are inclined to randomly aggregate on solid surfaces. Recently, a solid/liquid/gas three-phase interface was used to guide the aggregation/growth of reaction products.

DOI: 10.1021/jacs.5b12728
J. Am. Chem. Soc. 2016, 138, 1727−1748

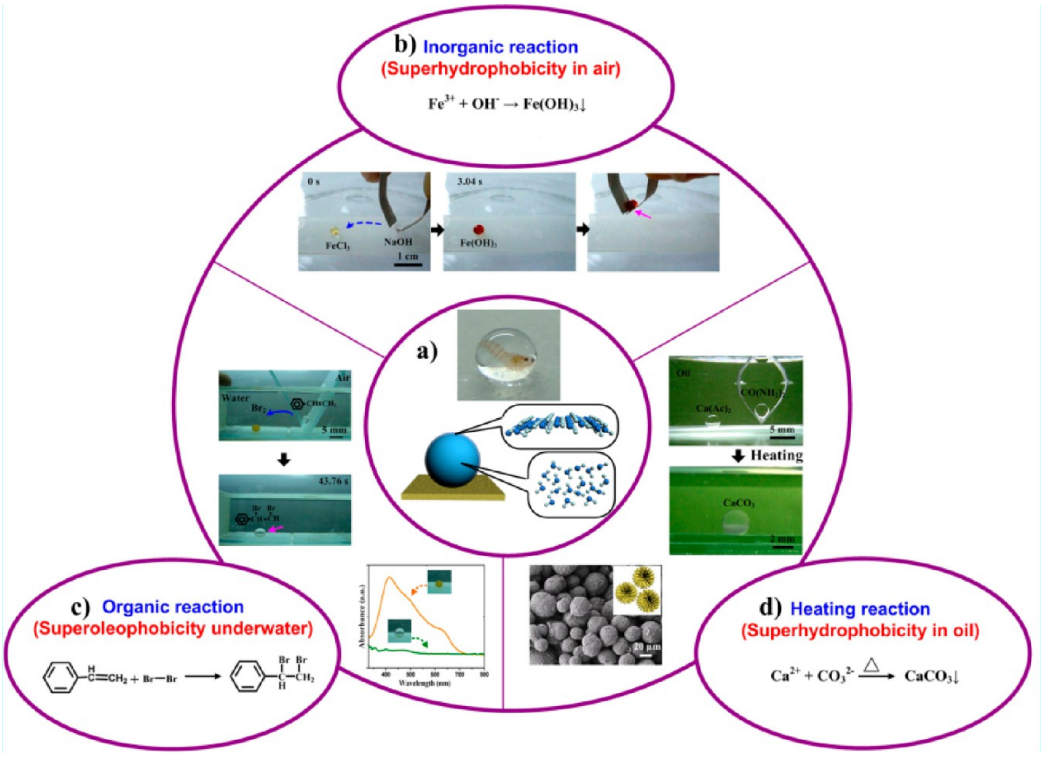

Figure 12. Effective usage of reactants and complete collection of products attributed to the low adhesion of superwettable surfaces. (a) Schematic illustration of manipulating the droplets to perform chemical reactions on the superhydrophobic/superoleophobic surfaces. (b) By building superhydrophobic tweezers and substrates in air, one aqueous droplet (containing $FeCl_3$) on the superhydrophobic surface could be coalesced with another droplet (containing NaOH) through the assistance of a pair of superhydrophobic tweezers, yielding a mixed droplet containing the product $Fe(OH)_3$. The products could be completely collected without any remaining residue. Reproduced with permission from ref 62. Copyright 2011 Springer. (c) If the tweezers and substrates are superoleophobic under water, an addition reaction could be performed without leaving a residue. Reproduced with permission from ref 58. Copyright 2011 The Royal Society of Chemistry. (d) By replacing an environment of water with silicone oil, a heatable and effective harvesting reaction was built by using under-oil superhydrophobic materials. Reproduced with permission from ref 63. Copyright 2012 The Royal Society of Chemistry.

Su et al. reported the controlled growth of gold architectures using superhydrophobic electrodes.[73] A conductive spindle-pillar-structured silicon substrate was fabricated by a laser-etching technique and exhibited superhydrophobicity after being coated with a monolayer of fluoride compounds. This anti-wetting surface was exposed to a 20 μL droplet of a $HAuCl_4$ solution, yielding a droplet-based electrochemical system (Figure 14a–c). Because of the air pockets trapped in the gaps of anti-wetting surfaces, an upward-facing meniscus was generated between two neighboring micropillars, which was confirmed by three-dimensional (3D) microscopic computed tomography. Following the gradual electro-reduction of the $[AuCl_4]^-$ ions inside the electrolyte, the gold particles began to aggregate from the solid/liquid/gas three-phase contact line rather than in the solid/liquid two-phase reaction region. Subsequently, the growth of gold architectures followed the upward liquid/gas interfaces caused by superhydrophobicity, forming a hollow gold microflower upon each micropillar.

Consequently, the authors performed another gas-participant precipitation reaction on these spindle-pillar-structured silicon substrates.[74] A Cd^{2+}-loading solution was exposed to a superhydrophobic pillar-structured substrate and placed in an atmosphere of H_2S gas at room temperature (Figure 14d,e). The H_2S gas dissolved into the electrolyte and reacted with the Cd^{2+} ions to yield CdS grains. The precipitation aggregated at the solid/liquid/gas three-phase contact line and continued along the upward-facing liquid/gas interfaces. After the reaction proceeded for approximately 20 min, hollow CdS architectures with sides reaching upward were formed on top of each pillar, and small grains of CdS could be found in the pillar gaps. Significantly, the direction of the superhydrophobicity-dominated solid/liquid/gas three-phase interface could be tailored by applying various pressures. In this case, the CdS architectures were able to grow upward, horizontally and downward. Furthermore, concentric microstructures could be generated by sequentially dropping liquids containing different metal ions onto the superhydrophobic pillar-structured substrates. For example, CdS microflower arrays could be fabricated by dropping a Cd^{2+}-loaded liquid onto the anti-wetting surfaces. A Pd^{2+}-loaded solution was then exposed to the CdS-loaded anti-wetting substrate and then placed in an H_2S gas atmosphere at room temperature. The H_2S gas dissolved into the electrolyte and then reacted with the Pd^{2+} ions to yield PdS grains. The reaction started at the CdS/electrolyte/air three-phase contact line rather than in the CdS/electrolyte two-phase reaction region. Therefore, CdS@PdS concentric microflowers were formed with an improved photon-harvesting ability.

3.1.3. Gas Networks with Contributions from Superhydrophobic Surfaces. The air pockets trapped in the superhydrophobic surfaces are not isolated but rather connected with each other and the atmosphere.[1] In this case, the gas networks not only help the surfaces repel the water but also provide an avenue for the transport of gas-phase reactants. Hatton's group reported regular spherical $CaCO_3$ precipitation patterns upon

DOI: 10.1021/jacs.5b12728
J. Am. Chem. Soc. 2016, 138, 1727–1748

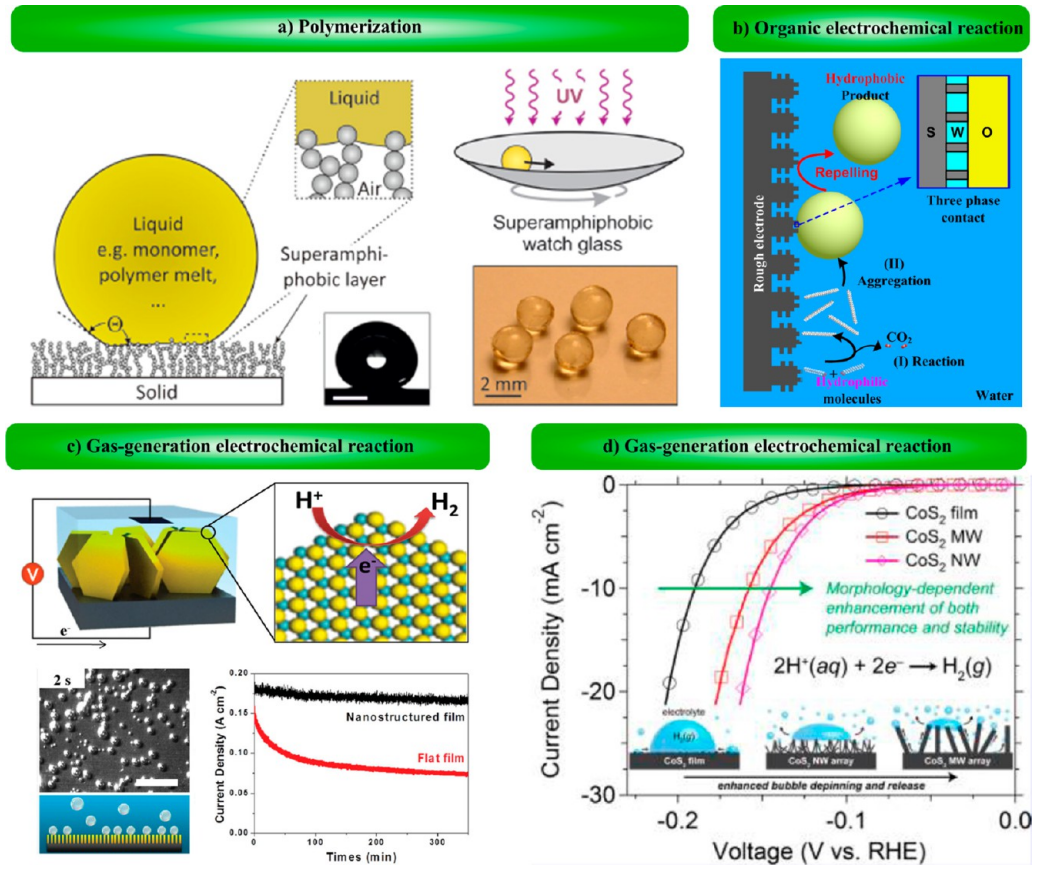

Figure 13. Unexpected chemical reactions existing upon superwettable surfaces. (a) The superamphiphobic surfaces allowed methacrylate to directly polymerize and form microspheres without the assistance of solvents. Reproduced with permission from ref 65. Copyright 2013 Wiley. (b) Underwater superoleophobic electrodes enabled the products to be repelled during the Kolbe electrochemical reaction, yielding a long and stable working life. (c) Underwater superaerophobic electrodes enabled the rapid release of bubbles, greatly advancing the high-efficiency generation of hydrogen. Reproduced with permission from ref 70. Copyright 2014 Wiley. (d) Rough underwater superaerophobic electrodes could prevent the adhesion of hydrogen bubbles to their surfaces. In this case, the performance and stability of the gas generation reaction could be enhanced accordingly. Reproduced with permission from ref 72. Copyright 2014 American Chemical Society.

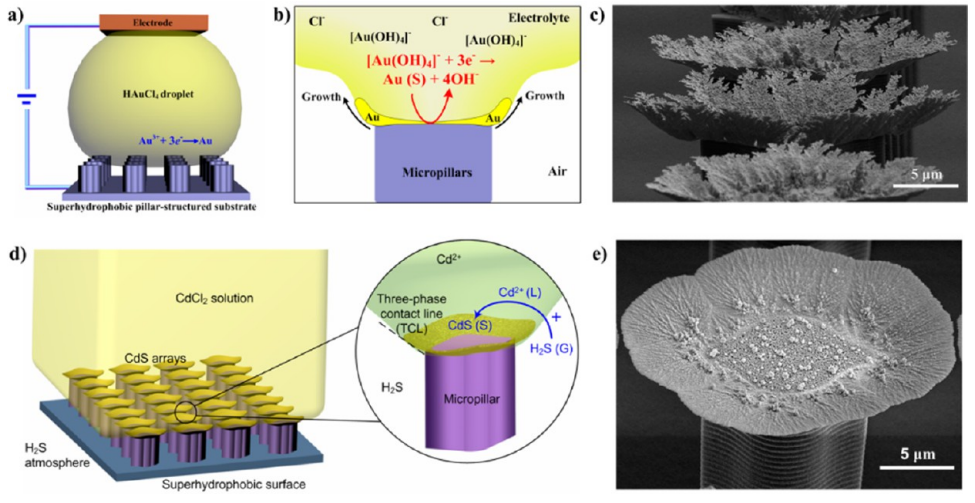

Figure 14. Three-phase contact line (TCL)-mediated interfacial chemical reactions. (a) Schematic illustration of a droplet-based electrochemical system on a superhydrophobic pillar-structured substrate. (b) Schematic illustration of the generation of gold microflowers on the micropillars. H^+ in the electrolyte was reduced to $[AuCl_4]^-$ as the gold nanoparticles aggregated along the solid/liquid/gas three-phase interface. (c) SEM images of electrodeposited Au structures viewed at 80°, showing upward hollow structures. Reproduced with permission from ref 73. Copyright 2013 Wiley. (d) Schematic illustration of a gas participation reaction system on a superhydrophobic pillar-structured substrate. The H_2S gas dissolved into the electrolyte and then reacted with the Cd^{2+} ions to precipitate CdS along the TCL. (e) Side-view SEM observations of the as-prepared interface-mediated CdS architecture. Reproduced with permission from ref 74. Copyright 2014 Wiley.

DOI: 10.1021/jacs.5b12728
J. Am. Chem. Soc. 2016, 138, 1727−1748

superhydrophobic post arrays.[75,76] Ca^{2+} ions were dissolved in the liquid on the anti-wetting posts while CO_2 gas was transported through the atmospherically connected post gaps. Different from traditional gas−liquid reactions that form continuous product films or precipitates, the precipitation reactions on these superhydrophobic surfaces were restricted (Figure 15a,b). A solid/liquid/gas three-phase interface existed

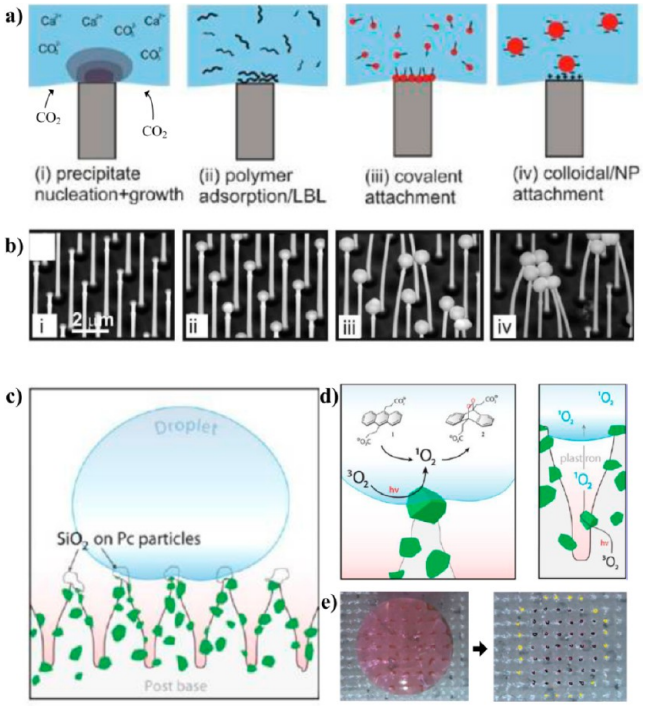

Figure 15. Gas network inside the gaps of superhydrophobic surfaces can transport gas-phase reactants to perform chemical reactions at the solid/liquid/gas three-phase interface. (a) Schematic illustration of $CaCO_3$ deposition on superhydrophobic pillar arrays. The pillar gaps provided the channels to continuously transport the CO_2 into the Cd^{2+}-loading liquid. As a result, spherical $CaCO_3$ deposition could be found on the top of each pillar. (b) Side-view SEM image of $CaCO_3$ deposition on micropillars within different reaction times. Reproduced with permission from ref 75. Copyright 2012 American Chemical Society. (c,d) Schematic illustration of a photo-oxidation reaction on Pt-loading superhydrophobic post arrays. The post gaps provided the channels to continuously transport the $^1O_2$ into the liquid. This $^1O_2$ reactant can react with 9,10-anthracene dipropionate dianion, yielding an organic reaction. (e) Optical image of the post array before/after contacting the dyed liquid. Reproduced with permission from ref 77. Copyright 2013 American Chemical Society.

on top of each post. CO_2 gas that passed through the superhydrophobicity-dominated gas network could diffuse through this three-phase interface to react with the Ca^{2+} in the electrolyte, yielding amorphous $CaCO_3$ microsphere arrays. The gas diffusion speed and droplet size both dominated the growth rate of the $CaCO_3$ architectures. The authors also demonstrated that these amorphous $CaCO_3$ microspheres could have the potential to favor drug release.

Recently, a triphasic photo-oxidation reaction on anti-wetting post arrays was reported (Figure 15c-e).[77,78] Highly active Pt particles were anchored to the tops of anti-wetting posts. Then, the superhydrophobicity-dominated gas network provided the channels needed to continuously transport O_2 from the atmosphere. The Pt particles transformed $^3O_2$ into $^1O_2$ in the post gaps and then dissolved the latter into the liquid. This $^1O_2$ reactant could react with 9,10-anthracene dipropionate dianion in a high-yield organic reaction. This study is a great example of the unique ability of superhydrophobic surfaces to offer a special route for $^1O_2$ transport. In traditional methods, the Pt particles are prevented from contacting $^3O_2$ when immersed in the water. As a result, the as-prepared $^1O_2$ was limited, yielding low reaction efficiency. Superhydrophobic surfaces, however, can allow effective contact between $^3O_2$ and the Pt particles through their atmospherically connected gas network. Therefore, the generation of $^1O_2$ was improved, producing an endoperoxide in 54−72% yield.

Aerobic bacteria, such as Saccharomycetes, require oxygen to perform their daily activities. However, they mostly live under water, which greatly restricts their collection of this gas. To address this challenge, Feng et al. employed superhydrophobic substrates to feed aerobic bacteria under nutrient fluids. Due to the atmospherically connected gas network existing on the superhydrophobic surfaces, the microbes could collect more oxygen than that on hydrophilic surfaces.[79] As a result, the production rate of their biochemical activities was improved by more than 100-fold.

The gas network of superhydrophobic surfaces can also be used to continuously absorb bubbles under water, allowing high-efficiency gaseous electrochemical reactions. In contrast to the underwater superaerophobic requirement of fuel cells,[70] a series of electrochemical reactions requires rapid contact between the electrodes and gas-phase reactants. Using underwater superaerophilic surfaces as electrodes, gas bubbles tend to absorb over the entire electrode area, allowing a fast and high-yield electrochemical reaction.

3.1.4. Superoleophilicity-Based Superslippery Surfaces. No chemical reactions have been observed to occur on "superslippery" surfaces in the literature to date. Because these types of surfaces are so unique, the authors forecast that they might lead to unexpected chemical behaviors in the future.

Recently, a novel superslippery surface has attracted much interest. Zhou et al. reported that diverse liquids, including water, glycerol, CH_2I_2, hexadecane, and rapeseed oil, were repelled by a porous alumina surface filled with hydrophobic perfluorooctyl acid.[80] The oil pockets played a key role in repelling water permeation, and the rough porosity optimized the anti-liquid property (Figure 16a,b). Aizenberg's group developed oil-infused superslippery surfaces in related biological studies.[81−85] Porous/textured surfaces were employed to trap the perfluorinated oil, allowing the water droplets to easily slip at a lower static CA and a lower sliding angle (Figure 16c,d).[81] If the rough substrates are replaced with flexible PDMS films or mesh supports, these low-adhesion materials can be used for promising applications in drag-reduced blood transport,[82] optical devices,[83] self-healing,[84] and oil−water separation,[85] among others.

These superslippery composite interfaces involve solids, oils, water, and air. To understand their basic mechanism, we begin with their derivation from under-oil superhydrophobic materials (Figure 8). Similar to under-oil water-repellent surfaces, the oil pockets are trapped inside the gaps of the superslippery materials, blocking the permeation of water. Because the environmental phase is air rather than oil, for superslippery materials, the static CA of water droplets is decreased due to the large surface tension. Due to the existence of water-repellent oil pockets in the gaps of rough surfaces, the water droplets can slip at a very tight sliding angle even though their static CA is quite low. Despite the tremendous advantages of these composite interfaces, two

DOI: 10.1021/jacs.5b12728
J. Am. Chem. Soc. 2016, 138, 1727−1748

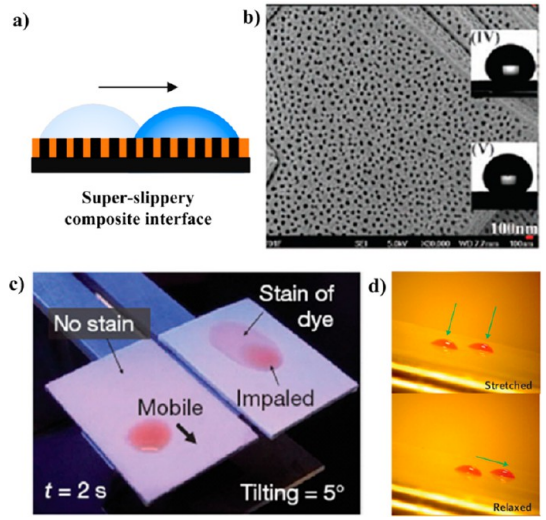

Figure 16. Superslippery surfaces are derived from under-oil superhydrophobic materials. (a) Schematic illustration showing the superslippery surfaces. Once the oil pockets fill the gaps in the rough solid surfaces, water droplets easily slip whether they are immersed under oil or simply in air. (b) Top view SEM observation of porous alumina surface with a pore size of ca. 40 nm. By filling the nanopores with hydrophobic perfluorooctyl acid, diverse liquids, including water, glycerol, CH_2I_2, hexadecane, and rapeseed oil, can be repelled by this surface. Reproduced with permission from ref 80. Copyright 2011 The Royal Society of Chemistry. (c) Digital image comparing the anti-wetting property between the slippery surface (left) and a normally superhydrophobic surface. The pentane droplets can slip quickly on the as-prepared liquid-filled surface but pin at the superhydrophobic surface. Reproduced with permission from ref 81. Copyright 2011 Nature Publishing Group. (d) Digital image of the bending-determined movement of droplets on the superslippery surfaces. Reproduced with permission from ref 83. Copyright 2013 Nature Publishing Group.

problems exist with this strategy: the easy mechanical peeling and the considerable evaporation of the oil pockets.

The functional oil pockets inside the surface gaps are easily removed by mechanical friction. As a result, their anti-wetting property will be reduced and even destroyed. To solve this problem, an organogel-based slippery surface has been proposed that exhibits both low-adhesion anti-wetting properties and robust mechanical resistance.[86] When polydimethylsiloxane films were immersed in toluene solvent, their swelling behavior allowed the organic oil to fill inside the network of molecular chains. In this case, the oil/polymer composite interfaces exhibited a low sliding angle of <5°. By controlling the morphology of the rough surfaces, anisotropic superslippery materials could also be fabricated.[87] Furthermore, temperature-dependent superslippery materials have been fabricated by replacing the fluoride oils trapped in the surface gaps with paraffin.[88] Because paraffin changes from a solid state to a liquid when heated above its melting point, water droplets on the composite surfaces can "superslip" or pin depending on the environmental temperature.

Most oils easily evaporate in air, yielding a loss of the anti-wetting ability of the composite interfaces. Therefore, using oils with a low rate of evaporation, such as ionic liquids, might overcome this drawback in the design of superslippery materials. Some primary attempts have been reported recently.[89]

3.1.5. Outlook: Fabrication of Thin Films Based on Superhydrophilicity. High adhesion caused by superhydrophilicity/superoleophilicity has been commonly considered a drawback of materials because liquids are inclined to leave a residue on these surfaces. Notably, the wetting nature is also useful when considered in a different way. For the fabrication of thin solid films through liquid-based techniques, including drop-casting, spinning, or dip-coating, the superwettable substrates might allow the rapid spreading of the liquids over the surfaces. Then, a thin solid film would be generated upon the evaporation of the organic solvents. Following this idea, a two-dimensional (2D) chemical reaction system can be built if droplets containing different reactants are sequentially dropped onto the substrates (Figure 17). The superwettability of the substrates allows effective mixing of different reactants in a restrictive 2D spacing, yielding multilayer/composite thin solid films.

3.2. Unique Crystallizations on Superwettable Interfaces. The evaporation of solvent in the suspension/solution can induce the crystallization of building blocks. The adhesive interaction between the liquid and solid substrates plays a key role in the assembled structures. Traditionally hydrophilic substrates can pin the droplets during their dewetting process. In this case, a "coffee ring"-shaped aggregation of the grains appears, yielding randomly positioned crystals. Interestingly, the air pocket "lubricating layer" on the superhydrophobic surfaces has been proven to effectively improve the solid/liquid interaction, allowing unexpected crystallization behaviors. Song and Wang et al. employed superhydrophobic polymer/nanoparticle composite substrates to restrict the crystallization of colloidal grains (Figure 18a).[90] The adhesion between the suspension and the substrates was tunable by tailoring the ratio of hydrophobic nanoparticles/polymer. Then, the shrinkage of the colloidal suspension was investigated on these surfaces. Following the reduction of adhesion from 269 to 156 μN, the crystallization of colloidal grains improved from a multi-crack to a crack-free state. Centimeter-scale colloidal crystallization with narrow stop bands of 12 nm was demonstrated on low-adhesion anti-wetting surfaces for the first time. Recently, the inkjet technique was used to locate droplets of a colloidal suspension onto similar low-adhesion surfaces.[91] The colloids could aggregate into spherical shapes, yielding wide-angle-visible structural colors (Figure 18c).

In addition to large-scale crystallizations, crystal patterns can also be built using superhydrophobic pillar-structured substrates. Jiang's group[92] and McCarthy's group[93] both found a unique crystal pattern behavior on hydrophobic pillar tops (Figure 18b). Superhydrophobic yet adhesive pillar arrays have been generated by modifying a layer of fluoride compounds onto laser-etching micropillars. A saline or colloidal suspension liquid was exposed to the anti-wetting surfaces and dewetted following the evaporation of water. In this case, a typical "U"-type liquid film was generated, allowing the existence of liquid bridges connecting neighboring micropillars. Because the viscosity of the saline or colloidal suspension was quite low, the liquid bridges were easy to break due to their poor mechanical strength. Thus, one microdroplet appeared upon each micropillar top. With the further evaporation of water, the solid/liquid/gas three-phase contact line of the microdroplets shrunk on the micropillar tops, allowing close packing of the building blocks to form high quality crystal arrays. By tailoring the concentration of the suspension or the size of the pillar top, the quantity of the building blocks changed accordingly.

3.3. Unique Microfabrication on Superwettable Interfaces. As mentioned in section 3.2, the liquid bridges caused by superhydrophobic pillar-structured surfaces are easily broken due to their poor strength after solvent evaporation. For example, replacing the building blocks inside the liquid bridges using polymers[94−97] and/or organic-capped nanoparticles[98] rather

DOI: 10.1021/jacs.5b12728
J. Am. Chem. Soc. 2016, 138, 1727−1748

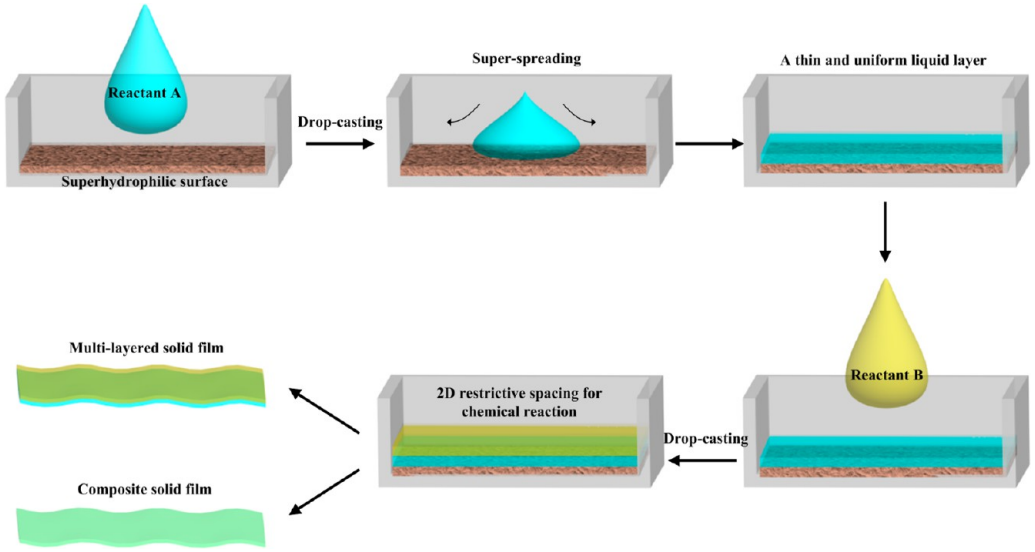

Figure 17. Superhydrophilicity/superoleophilicity-mediated ultrathin 2D restrictive spacing for chemical reactions. By drop-casting a liquid droplet on a superhydrophilic surface in a closed vessel, the liquid spreads quickly over the entire area of the substrate. A thin and uniform liquid film was generated. Then, a restrictive 2D spacing for chemical reactions can be generated by drop-casting another droplet containing different reactants onto this liquid film. Following the evaporation of the aqueous/organic solvents, a thin multilayer/composite solid film will be generated accordingly.

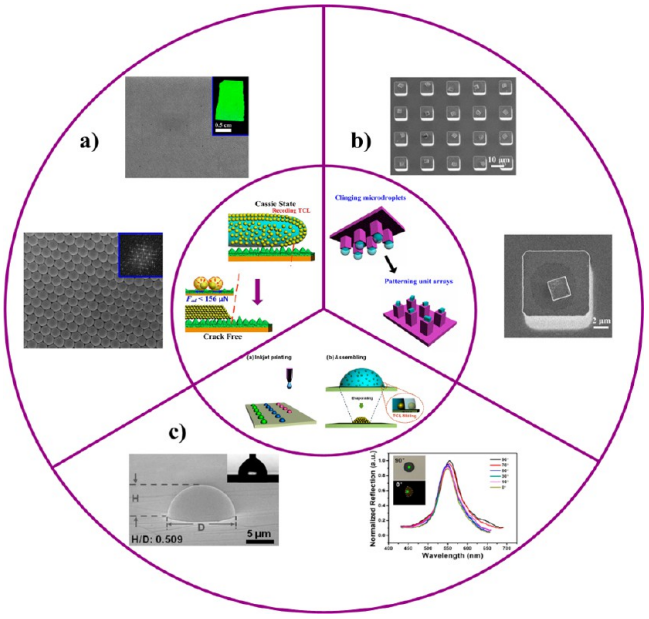

Figure 18. High-quality crystallization on superhydrophobic surfaces. (a) Schematic illustration of colloidal photonic crystals assembled on a superhydrophobic substrate. The latex particles assemble on the surface of the suspension and then shrink with the evaporation of the solvent. Large-scale, crack-free colloidal crystals were obtained on a superhydrophobic substrate. SEM images of large-scale, crack-free colloidal crystals. Reproduced with permission from ref 90. Copyright 2012 American Chemical Society. (b) Schematic illustration of the droplet dewetting process on superhydrophobic pillar-structured substrates. Following the evaporation of water, a microdroplet existed on the top of each pillar, yielding well-defined crystal arrays. SEM images of crystal arrays generated by diverse concentrations and pillar sizes. Reproduced with permission from ref 92. Copyright 2011 Wiley. (c) Schematic illustration of droplets of a colloidal suspension on the low-adhesion surfaces. The colloids could aggregate into spherical shapes, yielding wide-angle-visible structural colors. Reproduced with permission from ref 91. Copyright 2014 Wiley.

than inorganic salts can maintain the morphology of the liquid bridges, yielding regular 1D assemblies of these building blocks (Figure 19a). Because the position, alignment direction, and density of the liquid bridges are tunable, the rational design of a 1D assembly of diverse nanoscale building blocks, including organic molecules, nanoparticles, or graphene sheets, is easy.

When a droplet of an aqueous 0.1 wt% calcein solution shrunk on a superhydrophobic pillar-structured substrate, regularly aligned calcein nanowire arrays were generated with strict orientations and precise positions.[99] By tailoring the shapes and positions of the micropillars, a "zigzag"-type small molecular nanowire pattern was formed. Subsequently, another droplet containing Nile red molecules was placed on the nanowire-loaded superhydrophobic surface. Due to the Rayleigh instability along the 1D nanostructures, bead-shaped calcein@Nile red nanowire arrays were fabricated.[100] Because an overlapping energy band existed between the donor core (calcein) and the acceptor sheathing layer (Nile red), fluorescence resonance energy transfer could occur inside of these bead-shaped 1D nanostructures, creating a chemical sensor to detect diverse molecules/ions (Figure 19b). When exposed to $Cd(NO_3)_2$, $C_4H_9NH_2$, or I_2, the beads and joint parts would emit different light/dark signals.

In addition to small molecules, oil-soluble polymers, such as dithienylthieno[3,2-*b*]thiophene−*N*-alkyl diketopyrrolopyrrole-based conjugated polymer, could also be aligned into oriented nanowire arrays through an "underwater superoleophobicity-mediated assembly" strategy (Figure 19c).[101] The functional polymer was dissolved in ortho-dichlorobenzene to form a liquid film on an underwater superoleophobic pillar-structured substrate. Following the evaporation of the organic solvent, regular polymeric nanowire arrays were generated with tunable alignment and positioning. These nanowire patterns could be integrated into flexible field-effect transistors, exhibiting an order of magnitude higher mobility compared with their thin-film counterpart. A regular molecular alignment restricted by the liquid bridges was the main cause of this improved mobility.

Gold nanoparticles capped by organic ligands were assembled into 1D architectures through this "liquid bridge-induced

DOI: 10.1021/jacs.5b12728
J. Am. Chem. Soc. 2016, 138, 1727−1748

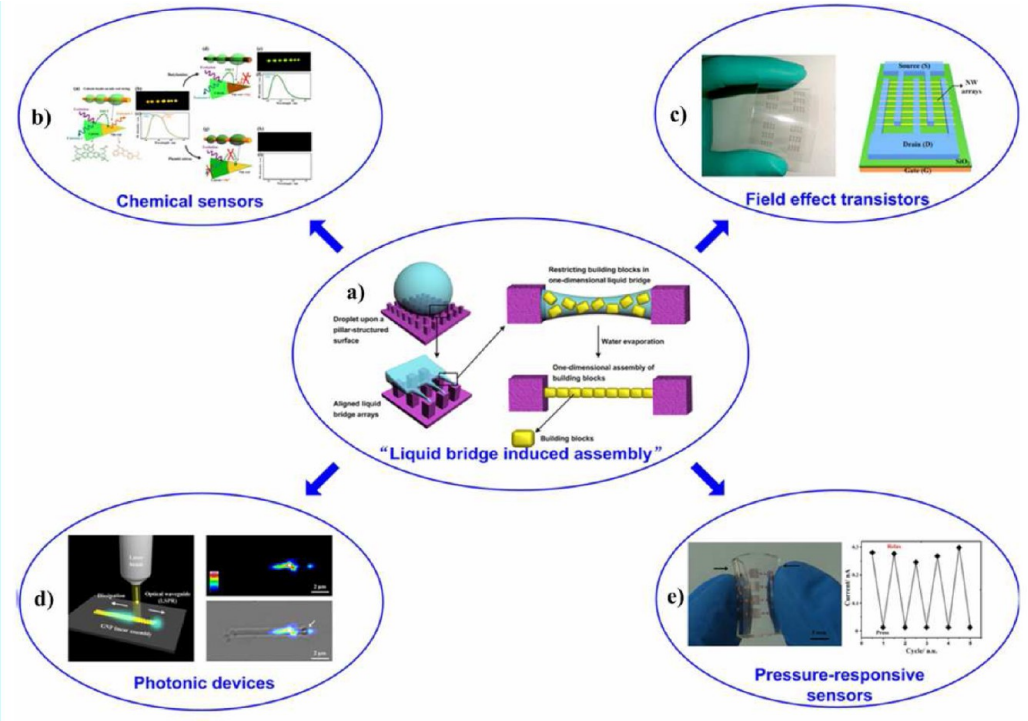

Figure 19. Liquid-bridge-induced 1D assembly dominated by superwettable surfaces. (a) Schematic illustration of the generation of liquid bridge arrays on superhydrophobic pillar-structured substrates. A typical "U"-type liquid film was generated, allowing the existence of liquid bridges connecting neighboring micropillars. With the evaporation of water, the building blocks inside the liquid bridges could be assembled in one direction with close packing. (b) By assembling ion-responsive small molecules into regular 1D patterns, a nanowire-based chemical sensor can be obtained. Reproduced with permission from ref 100. Copyright 2013 The Royal Society of Chemistry. (c) By assembling semiconductor materials into regular 1D patterns, a nanowire-based field effect transistor can be fabricated. Reproduced with permission from ref 101. Copyright 2013 Wiley. (d) By arranging gold nanoparticles in regular 1D patterns, the directional transport of photons appeared. Reproduced with permission from ref 102. Copyright 2013 Wiley. (e) By assembling graphene sheets in a regular pattern, a flexible sensor for monitoring human behavior can be fabricated. Reproduced with permission from ref 104. Copyright 2014 Wiley.

assembly" strategy.[102] Photons were coupled with the plasmonic resonances of gold nanoparticle chains (Figure 19d). Thus, the light exhibited directional transport along the 1D nanostructures. Furthermore, diverse nanoscale building blocks, such as 3−5 nm CdTe quantum dots, 40−50 nm silver nanoparticles, and 300−800 nm polystyrene beads, could be assembled in precise patterns through the liquid bridge-induced assembly strategy.[103] Even 2D graphene sheets were assembled into regular patterns and showed potential in flexible mechanical sensors (Figure 19e).[104]

Very recently, guided physical vapor transport was proposed to generate highly positioned, aligned single-crystal microwires (Figure 20a−c).[105] Aligned micropillars with diverse wettabilities (superhydrophilicity on the tops and superhydrophilicity on the sidewalls) on the top and sidewall regions have been used to guide the 3D dewetting of organic liquids. Therefore, strictly oriented single-crystal microwires grew at the corners of the micropillars and were easily transferred onto flexible plastic films. The positioning of organic liquids would be dominated by this 3D wettability difference accordingly, leading to diverse microwire patterns (Figure 20d−f).

3.4. Other Physical-Chemical Behaviors on Superwettable Surfaces. *3.4.1. Ion-Sensitive Superwettable Surfaces.* Ions can affect the interactions between liquid and solid surfaces, yielding tunable yet reversible wettabilities. For example, Gellman and Abbott et al. reported that the protonation of amine groups increased the strength of hydrophobic interactions, whereas guanidinium groups decreased the hydrophobic interactions over a wide range of pH values (Figure 21a).[106,107] By tailoring the ion species and/or concentration, the interactions between the liquid and solid surfaces changed, leading to tunable underwater superoleophobicity. Wang et al. generated polyelectrolyte multilayers consisting of alternative of poly(diallyldimethylammonium) chloride (PDDA) and poly(styrenesulfonate) (PSS).[108] For PDDA-capped surfaces, the surface hydrophilicity was maintained by vertically aligned quaternary amine groups. In contrast, the PSS-capped surfaces exhibited tunable oil repellency in water with contributions from the benzenesulfonate groups with an anisotropic configuration.

H^+ ions have been used to tailor the interfacial interaction between oil and aqueous electrolytes, yielding switchable underwater superwettability. Jiang et al. reported a solid-phase-independent wettability change by tailoring the pH of the water (Figure 21b).[109] The oil droplets are mostly Lewis acids, and the hydroxide ions in water are Lewis bases. In this case, by tuning the pH, the Lewis acid−base interactions appear or disappear at the oil−water interface, yielding underwater oleophilic and superoleophobic states. Sun et al. also reported a pH-dependent underwater superwettability.[110,111] Hydrophilic carboxylic or hydroxyl groups and hydrophobic alkyl groups were alternatively modified on the solid surfaces. Then, the change in pH in the electrolyte would affect the Lewis acid−base interactions at the oil−solid interface. Therefore, the oil CA changed from 162° to ~0° under water.

In addition to superoleophobicity/superoleophilicity under water, a controlled switch between the diverse components of the superwettability system (Figure 8) is also possible. The concept

DOI: 10.1021/jacs.5b12728
J. Am. Chem. Soc. 2016, 138, 1727−1748

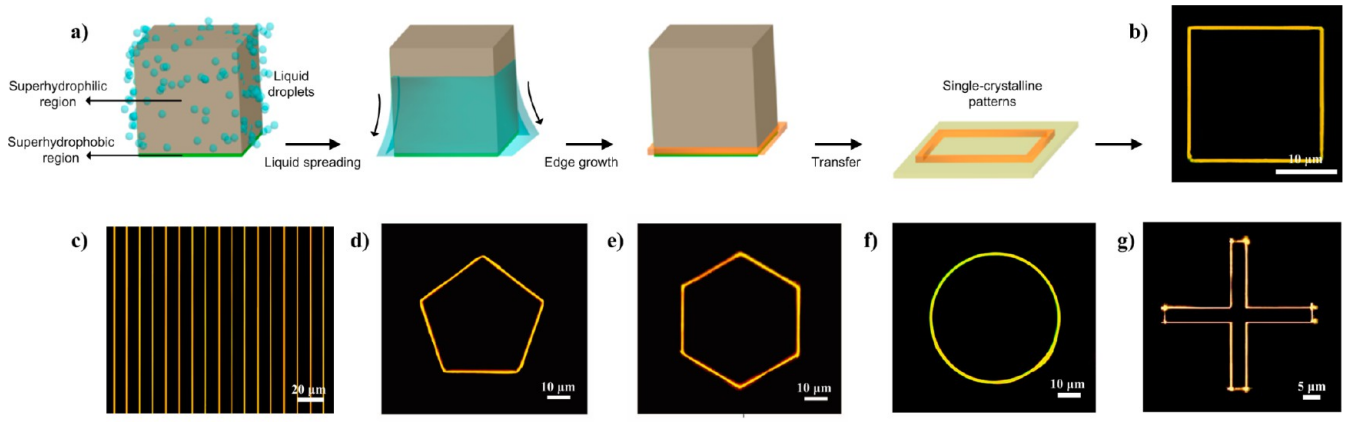

Figure 20. Three-dimensional dewetting-mediated microwire patterns with strict alignment and positioning. Schematic illustrations show the dewetting process of organic liquids along the pillar sidewalls. (a) Numerous droplets of organic liquids adhered to the sidewalls of the superhydrophilic pillar. Then, the liquid would spread and dewet along the pillar sidewalls toward the superhydrophobic bottom. Due to the wettability difference between the pillar sidewalls (superhydrophilicity) and bottoms (superhydrophobicity), the organic liquids were located at the bottom edges of the pillar sidewalls, yielding aligned microwire patterns. Dark-field fluorescent micrographs of single (b) square, (c) line, (d) pentagonal, (e) hexagonal, (f) circle, and (g) Latin cross-shaped 9,10-bis(phenylethynyl)anthracene wires, demonstrating that organic, 1D structures can be grown at precise internal angles of 90° (square), 108° (pentagon), and 120° (hexagon). Reproduced with permission from ref 105. Copyright 2015 Nature Publishing Group.

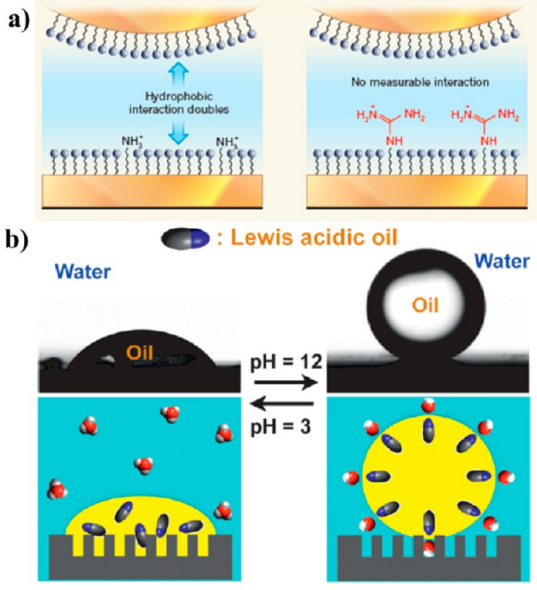

Figure 21. Ion-sensitive superwettable surfaces under water. (a) Schematic illustration showing that amine groups on the surfaces increased the strength of the hydrophobic interactions, whereas guanidinium groups decreased the hydrophobic interactions. Reproduced with permission from ref 107. Copyright 2015 Nature Publishing Group. (b) Reversible wettability can be attained for an underwater oil droplet by tailoring the H^+ concentration of the surrounding environment. An oleophilic/superoleophobic reversible surface can be generated for the Lewis acid oil through the contributed of Lewis acid−base interactions existing at the interface between the water and solid surface. Reproduced with permission from ref 109. Copyright 2012 Wiley.

of smart superwettability is only in its infancy. By altering the type of matter used, such as replacing the water/oil droplets with bubbles, a reversible switch between underwater/-oil superaerophobicity/superaerophilicity can be achieved. By changing the environmental phase from water to oil, a reversible switch between under-oil superhydrophobicity/superhydrophilicity is also promising. Furthermore, the oil can be extended to ionic liquids, metallic liquids, magnetic liquids, liquid crystals, aqueous chemical mixtures, or other organic liquids (Figure 9), and the external stimuli can also be adapted to optical, electrical, magnetic, or other physical candidates. In summary, the study of smart superwettability will grow and attract more attention from researchers in diverse fields.

3.4.2. Superwettability at Extreme Temperatures. a. High Temperatures (>100 °C). Heating water on solid surfaces is very common in both humans' daily lives and industrial activities. Thermal energy passes through the solid surface to the water, allowing the liquid to nucleate and boil. Thus, several bubbles anchor to the solid surface, yielding a stable vapor film as this ongoing process progresses, which is known as film boiling or the Leidenfrost phenomenon.[112] Tailoring the wettability of the solid surfaces greatly changes the Leidenfrost phenomenon.

To study the relationship between surface wettability and the Leidenfrost phenomenon, four types of surfaces—flat, nanowire-array-structured, micropillar-structured, and two-tier rough silicon micro-/nanowafers—were fabricated by lithography and/or chemical etching.[113] Two types of surface chemical compositions, such as hydrophobic fluoroalkylsilane molecules and hydrophilic silicon atoms, were formed with/without chemical treatment. Then, the temperature-dependent Leidenfrost phenomenon was carefully investigated using these surfaces with eight types of wettabilities. A Leidenfrost transition temperature of nearly 100 °C could be attained upon superhydrophilic, hydrophilic and hydrophobic surfaces. Interestingly, the Leidenfrost transition completely disappeared on the superhydrophobic samples (Figure 22a). The gas-lubricating layer trapped in the gaps of the rough solid surface contributed to this unusual phenomenon. Buongiorno et al. performed a similar study using micropillar-structured surfaces.[114] Mudawar et al. also investigated the dependence of the chemical composition and surface morphology of the Leidenfrost phenomenon.[115]

In addition to vertically aligned nanowires, recently, the surfaces of tilting silicon nanowires (TSNWs) were found to exhibit directional drop transport (Figure 22b).[116] When heated at 350 °C, bubbles could be generated in the bottom part of the microstructures. Following the guidance of TSNWs, gas bubbles increased, allowing water droplets to bounce along in the direction of the TSNWs. Therefore, the directional droplet

DOI: 10.1021/jacs.5b12728
J. Am. Chem. Soc. 2016, 138, 1727−1748

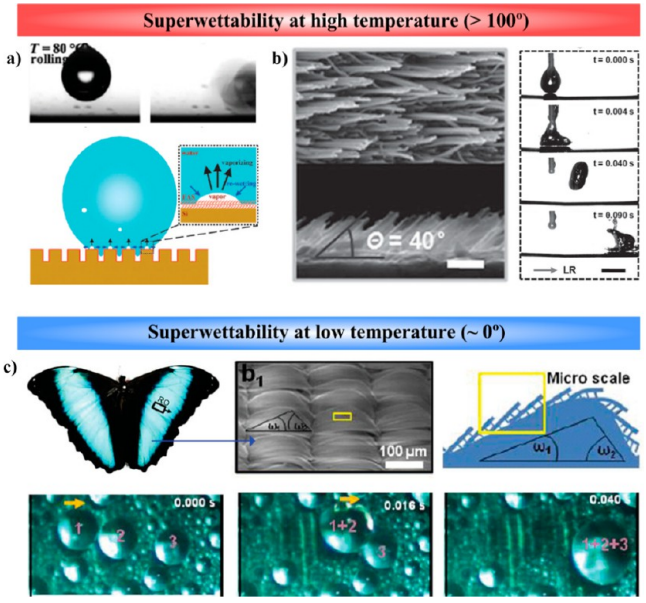

Figure 22. Superwettability at extreme temperatures. (a) Digital images recording the wetting/bouncing behavior of water droplets on a superhydrophobic silicon two-tier rough micro-/nanosurface at high temperature. Due to the existence of air pockets trapped insides structural gaps, droplets cannot bounce accordingly. The Leidenfrost effect can be improved by the superwettable surfaces. Reproduced with permission from ref 113. Copyright 2011 Wiley. (b) Left: top and cross-sectional view SEM images of tilting silicon nanowire surfaces. Right: digital images recording the explosion and directional bounce of drops deposited on the surface. Reproduced with permission from ref 116. Copyright 2014 Wiley. (c) Controlled dropwise condensation on superwettable surfaces. By tailoring the geometry and arrangement of microstructures, condensed droplets can move directionally. Top: digital image recording the wings of a *Morpho deidamia* butterfly, in which a directional micro-/nano-ratchet-like structure can be observed. Bottom: top view images recording the directional transport of fog drops on a static butterfly wing. Yellow arrows indicate the direction of movement of condensed droplets. Reproduced with permission from ref 118. Copyright 2014 American Chemical Society.

motion was controlled by tailoring the titling angles of the nanowires.

b. Low Temperatures (~0 °C). Dropwise condensation is a common phenomenon that occurs when a vapor makes contact with a supercooled surface. Generally, the vapor transfers to the water droplets on the solid surfaces. Then, the wettability of the surfaces determines the rolling away or pinning of these droplets. In nature, some organisms collect drinking water from humid air by setting droplets into motion.[117] In industrial applications, condensed droplets usually pin on the heat exchangers, leading to poor thermal conductance and reduced heat transfer efficiency. Thus, it is a great challenge to improve the dropwise condensation on solid surfaces. Learning from nature, tailoring the wettability is a simple yet effective process.

The Stenocara beetle in the Namib Desert is an incredible creature that can collect microdroplets from fog using their backs, which are covered with hydrophilic/hydrophobic patterns.[117] Hydrophilic regions allow the condensation of microdroplets while hydrophobic domains guide the directional movement of these drops. The transport of the condensed fog drops is random and mostly dominated by gravity on the hydrophilic/hydrophobic patterned backs of the Stenocara beetles. In contrast, the wings of *Morpho deidamia* butterflies exhibit an effective strategy for the directional transport of condensed fog drops.[118] The butterfly wings consist of a unique ratchet-like micro-/nanostructure. Scales covered by porous asymmetric ridges are regularly arranged (Figure 22c). Due to this unique microstructure, the water droplets randomly condense on the butterfly wings, then coalesce and easily roll away along the RO direction. Asymmetric microstructures and the coalescence of fog drops due to the hydrophobic ratchet-like structures are two key factors in determining this directional droplet motion. As a result, the butterflies easily remove the condensed droplets by vibrating their wings at a low frequency.

Based on the research on superwettability at extreme temperatures, controllable droplet ejection can be obtained by covering surfaces with stimuli-responsive molecules. In this case, the interactions between the liquid and solid surfaces change according to optical, electrical, magnetic, or other physical stimuli, allowing the droplets to jump out or pin on only the solid substrates at extreme temperatures.

3.4.3. 1D Superwettability. a. Fiber-Based Superwettability. Spider silk is a unique natural example of harvesting water droplets from mist.[119] Periodic spindle knots and joints were alternatively arranged along spider silk after a wet-rebuilt process (Figure 23a,b). Random nanofibers appeared on the knots, and aligned nanofibers existed on the joint regions. Due to the differences in the surface microstructures, the wettability of the knots tended to be more hydrophilic, yielding directional movement of the droplets from the joints toward the knot areas. Another biological example is the superwettability-based fog collection of cactus spines (Figure 23c,d).[120,121] Droplet motion on the spine is directional due to its multistructure. The small droplets first condense randomly on the spine, then coalesce and move toward the wider grooves due to Laplace pressure. Learning from these organisms, the liquid harvesting and collection abilities of artificial spider silk and cactus spines have been mimicked.[122] Controlling the wettability of the knot and joint regions of artificial spider silk drove the condensed droplets toward or away from the joint areas. Furthermore, through the modification of thermoresponsive or photosensitive polymers on the knots of artificial spider silk, the droplets' movements were controlled by changing the external stimuli.[123] Recently, condensed droplets were reported to move toward one direction when gradient[124] or multilevel[125] spindle knots were generated on artificial spider silk.

Bioinspired fibers with superwettability can be applied in many fields, including smart catalysis, filtration, and sensing (Figure 23e–j). For example, smart catalysis can be performed on the spindle knot by a cycle of two processes. One is the directional transport of the reactant droplets toward the catalysis-containing spindle knot, and the other is the rapid removal of the obtained products from the spindle knot.[126] Moreover, small materials in the air (e.g., particles) can be harvested by tiny liquid droplets and further concentrated or filtered on the bioinspired spider silk, leading to ultra-low-concentration sensors.

b. Superwettability-Based Nanochannels. Asymmetric wettability can also be built inside 1D microchannels. For example, Jiang and Tian et al. developed bioinspired ionic channels with a unique cooperative pH-responsive double gate.[127] Two opposite pH-responsive polyelectrolytes, poly(vinylpyridine) (PVP) and poly(acrylic acid) (PAA), were separately modified onto the two tip sides of the cigar-shaped nanochannel by a well developed asymmetric modification method (Figure 24e). By tailoring the pH of the electrolytes exposed to both sides of the channels, the wettabilities along the nanochannels changed greatly.

DOI: 10.1021/jacs.5b12728
J. Am. Chem. Soc. 2016, 138, 1727–1748

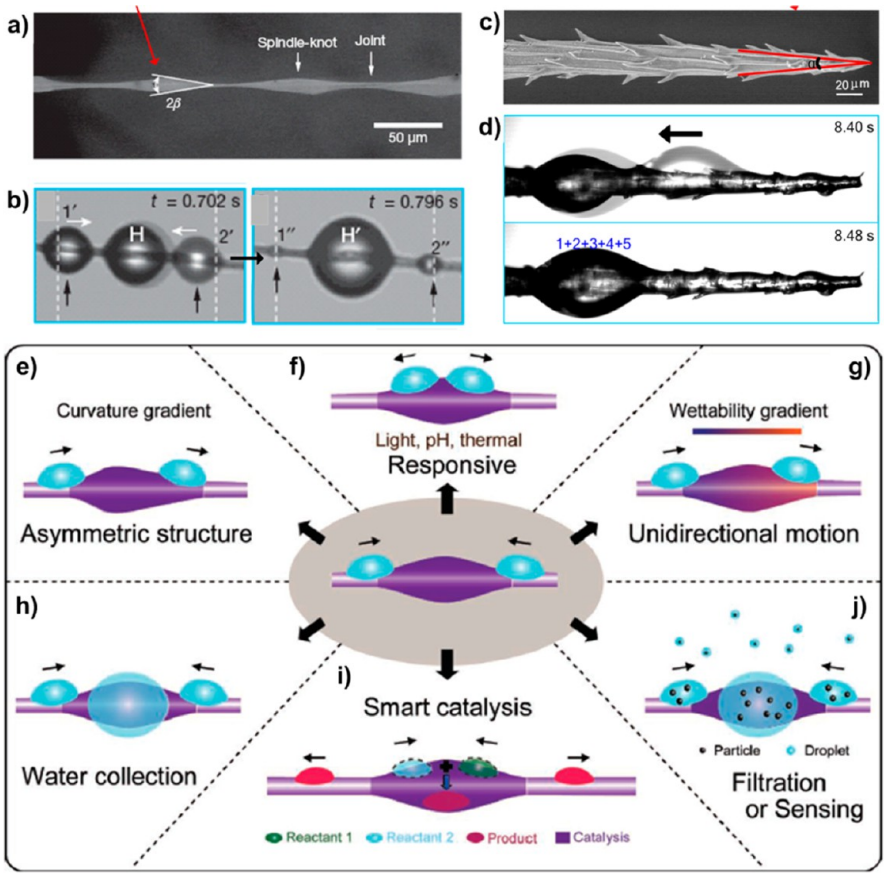

Figure 23. Schematic illustration of promising concepts and applications of bioinspired functional fibers with superwettability. (a) SEM image of spider silk. The spindle-arranged spider silk can drive water droplet movement toward a controlled direction. (b) Optical image of water droplets on spider silk. Smaller droplets condensed randomly on the knots and joints and then coalesced to larger droplets on only the knots. Reproduced with permission from ref 119. Copyright 2009 Nature Publishing Group. (c) SEM observation of a spine from the *O. microdasys* stem. (d) Directional droplet motion on the spine. The smaller droplets first condensed randomly on the spine and then coalesced and moved toward the wider part due to Laplace pressure. Reproduced with permission from ref 120. Copyright 2012 Nature Publishing Group. These bioinspired structures can lead to further promising applications in diverse fields. (e) Controllable motion of water droplets appears by designing asymmetric structures or g) wettability gradients on the spindle-knots. (f) Stimuli-responsive molecules can be modified on the spindle-knots, yielding a tunable direction of movement of the droplets based on light, pH, or thermal stimuli. h) High-efficiency water collection generated using the directional collection of small drops. (i) Smart catalysis system consisting of two mechanisms: (i) directional transport of reactant droplets toward the spindle-knot that contains catalysis; (ii) rapid removal of product droplets away from the spindle-knot. j) Concentration of a small amount of materials in the air through recycled droplet aggregation and evaporation on the spindle-knot. Reproduced with permission from ref 122. Copyright 2012 Wiley.

For example, a gradient from hydrophobicity (PVP-modified tip) to hydrophilicity (PAA-modified tip) occurred when the pH was 2.8. In contrast, the gradient was reversed by increasing the pH to 10.0. In this case, the K^+ and Cl^- ions could be selectively transported by the change in asymmetric wettability inside the nanochannels. Furthermore, asymmetric wettability inside nanochannels has also been reported.[128] Ion-responsive G4 DNA motors and pH-sensitive C4 DNA motors were grafted onto the inside surface of nanochannels. By tailoring the ion concentration in the G4 DNA-modified tip and the pH in the C4 DNA-covered tip, asymmetric wettability appeared, allowing the selective transport of ions or water. More details on superwettability-based ion channels can be found in several comprehensive reviews.[129−136]

In addition to the ability to control ion transport by the opening/closing of the gates, artificial nanochannels could have several promising applications, especially in energy conversion. Inspired by retina, Jiang et al. reported a novel energy conversion system to obtain electric signals driven by photoenergy (Figure 24f).[137] Another example is a study based on electric eels, an animal that can generate up to 600 V within milliseconds of encountering danger. Na^+/K^+ ion pumps are the main key to this unique ability of these organisms. Therefore, negatively charged nanochannels were fabricated to transfer ion concentration-gradient-induced chemical energy to electrical energy (Figure 24g).[138] Furthermore, nanoporous composite membranes consisting of mesoporous carbon and anodic aluminum oxide were proposed to enhance the energy-conversion output (Figure 24h),[139] yielding a high output of 3.46 W/m^2. In addition to a salt gradient, pressure can also be transferred to electronic energy by 2D layered graphene hydrogel membranes (Figure 24i).[140] This simple design could be used as insoles in shoes to continually generate output power when people walk.

4. CONCLUSIONS AND PERSPECTIVES

In this Perspective, we summarized the recent progress in "superwettability systems" and the related chemistry. Fundamental rules for building superwettable materials and exploiting new avenues to facilitate traditional chemistry have been discussed. The superwettability system can be extended to 1D/2D/3D fibrous/porous structures, allowing opposite wettabilities when

DOI: 10.1021/jacs.5b12728
J. Am. Chem. Soc. 2016, 138, 1727−1748

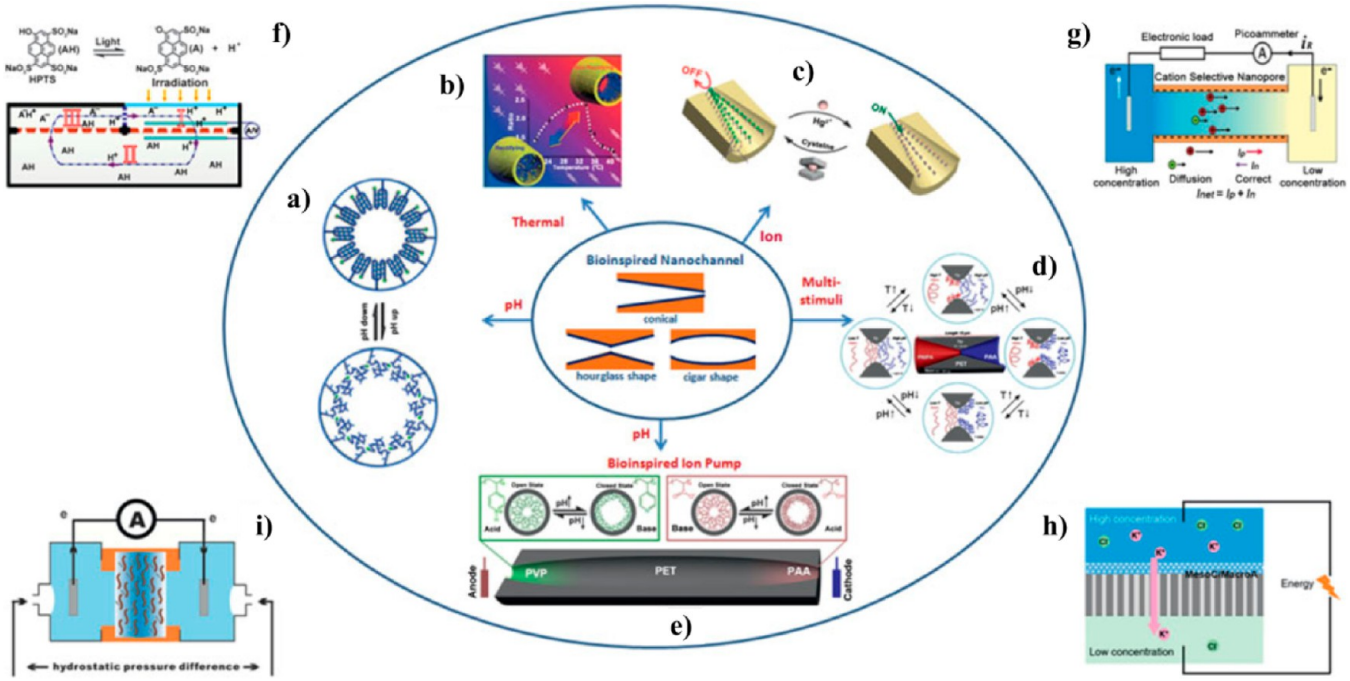

Figure 24. Superwettability-based nanochannels (middle) and their applications (surrounding). Bioinspired nanochannels with different shapes. (a) Single conical polymeric nanochannels (SPNs) covered by pH-sensitive i-motif DNA. Reproduced with permission from ref 133. Copyright 2009 American Chemical Society. (b) Thermal-responsive smart ion channels generated by coating conical SPN with poly(*N*-isopropylacrylamide) (PNIPAM). Reproduced with permission from ref 134. Copyright 2010 Wiley. (c) Mercury(II)-sensitive ion channels from modification of 50-thiol-ended T-rich single-stranded DNA onto Au-coated conical SPN. Reproduced with permission from ref 135. Copyright 2013 The Royal Society of Chemistry. (d) pH and thermal dual responsive ion channels through asymmetric modification with poly(acrylic acid) (PAA) and PNIPAM at the two sides of hourglass-shaped SPN, respectively. Reproduced with permission from ref 136. Copyright 2010 American Chemical Society. (e) Bioinspired ion and pH-sensitive pump. Reproduced with permission from ref 127. Copyright 2013 American Chemical Society. (f) Energy conversion system inspired by the retina. The photo energy can be converted into electrical signals through the DNA-covered nanochannels and photosensitive acid/base molecules. Reproduced with permission from ref 137. Copyright 2009 Wiley. (g) Energy-conversion device inspired electric eels. Chemical energy can be converted into electrical energy by the negatively charged nanochannels. Reproduced with permission from ref 138. Copyright 2010 Wiley. (h) Energy conversion membranes based on a salinity gradient. Mesoporous carbon was combined with anodic aluminum oxide. Reproduced with permission from ref 139. Copyright 2014 American Chemical Society. Reproduced with permission from ref 140. Copyright 2013 Wiley.

exposed to diverse external stimuli, such as temperature, light, electricity, pH, ions, or target molecules. We expect that more researchers will become interested in this field and further the connection between superwettability and chemistry. For example, Figure 8 does not represent the final state of the superwettability system because the oil phase can consist of diverse species, as shown in Figure 6. With a deep understanding of the interaction among the solid, liquid and gas phases, more unexpected research on superwettable states and their unique chemical behaviors will be found. Although we have summarized some recent research related to superwettable materials, we would rather regard this Perspective as an opening remark than a conclusive one, because superwettability-based research remains promising and attractive. There is still undoubtedly a broad space for the development of superwettability-based chemistry toward new materials and optical/electronic applications.

AUTHOR INFORMATION

Corresponding Author

*jianglei@iccas.ac.cn

Notes

The authors declare no competing financial interest.

ACKNOWLEDGMENTS

This research is supported by the National Research Fund for Fundamental Key Projects (2013CB933000), the National Natural Science Foundation of China (21121001, 91127025), and Australian Research Council's Discovery Early Career Researcher Award (DECRA) funding scheme (DE140100541).

REFERENCES

(1) Wang, S. T.; Liu, K. S.; Yao, X.; Jiang, L. *Chem. Rev.* **2015**, *115*, 8230−8293.
(2) Liu, K. S.; Yao, X.; Jiang, L. *Chem. Soc. Rev.* **2010**, *39*, 3240−3255.
(3) Liu, K. S.; Cao, M. Y.; Fujishima, A.; Jiang, L. *Chem. Rev.* **2014**, *114*, 10044−10094.
(4) Young, T. *Philos. Trans. R. Soc. London* **1805**, *95*, 65−87.
(5) Ollivier, H. *Ann. Chim. Phys.* **1907**, *10*, 229.
(6) Ollivier, H. *Ann. Chim. Phys.* **1907**, *10*, 289.
(7) Bartell, F. E.; Shepard, J. W. *J. Phys. Chem.* **1953**, *57*, 211−215.
(8) Li, H. J.; Wang, X. B.; Song, Y. L.; Liu, Y. Q.; Li, Q. S.; Jiang, L.; Zhu, D. B. *Angew. Chem., Int. Ed.* **2001**, *40*, 1743−1746.
(9) Onda, T.; Shibuichi, S.; Satoh, N.; Tsujii, K. *Langmuir* **1996**, *12*, 2125−2127.
(10) Chen, W.; Fadeev, A. Y.; Hsieh, M. C.; Öner, D.; Youngblood, J.; McCarthy, T. J. *Langmuir* **1999**, *15*, 3395−3399.
(11) Lafuma, A.; Quéré, D. *Nat. Mater.* **2003**, *2*, 457−460.
(12) Barthlott, W.; Neinhuis, C. *Planta* **1997**, *202*, 1−8.
(13) Tian, Y.; Su, B.; Jiang, L. *Adv. Mater.* **2014**, *26*, 6872−6897.
(14) Feng, L.; Li, S. H.; Li, Y. S.; Li, H. J.; Zhang, L. J.; Zhai, J.; Song, Y. L.; Liu, B. Q.; Jiang, L.; Zhu, D. B. *Adv. Mater.* **2002**, *14*, 1857−1860.
(15) Koch, K.; Bhushan, B.; Jung, Y. C.; Barthlott, W. *Soft Matter* **2009**, *5*, 1386−1393.

DOI: 10.1021/jacs.5b12728
J. Am. Chem. Soc. 2016, 138, 1727−1748

(16) Verho, T.; Korhonen, J. T.; Sainiemi, L.; Jokinen, V.; Bower, C.; Franze, K.; Franssila, S.; Andrew, P.; Ikkala, O.; Ras, R. H. A. *Proc. Natl. Acad. Sci. U. S. A.* **2012**, *109*, 10210−10213.
(17) Feder, D. O.; Koontz, D. E. *Symposium on cleaning of electronic device components and materials*. American Society for Testing Materials, 1959, *246*, p 136.
(18) Kozlova, S. A.; Kirik, S. D. *Microporous Mesoporous Mater.* **2010**, *133*, 124−133.
(19) Wang, R.; Hashimoto, K.; Fujishima, A.; Chikuni, M.; Kojima, E.; Kitamura, A.; Shimohigoshi, M.; Watanabe, T. *Nature* **1997**, *388*, 431−432.
(20) Liu, M. J.; Wang, S. T.; Wei, Z. X.; Song, Y. L.; Jiang, L. *Adv. Mater.* **2009**, *21*, 665−669.
(21) Bhushan, B.; Jung, Y. C. *Prog. Mater. Sci.* **2011**, *56*, 1−108.
(22) Darmanin, T.; de Givenchy, E. T.; Amigoni, S.; Guittard, F. *Adv. Mater.* **2013**, *25*, 1378−1394.
(23) Liu, M. J.; Jiang, L. *Adv. Funct. Mater.* **2010**, *20*, 3753−3764.
(24) Coghill, W. H.; Anderson, C. O. *U. S. Bur. Mines Technol. Pap.* **1923**, *262*, 47.
(25) Gao, X. F.; Jiang, L. *Nature* **2004**, *432*, 36−36.
(26) Gao, X. F.; Yan, X.; Yao, X.; Xu, L.; Zhang, K.; Zhang, J. H.; Yang, B.; Jiang, L. *Adv. Mater.* **2007**, *19*, 2213−2217.
(27) Zheng, Y. M.; Gao, X. F.; Jiang, L. *Soft Matter* **2007**, *3*, 178−182.
(28) Autumn, K.; Sitti, M.; Liang, Y. C. A.; Peattie, A. M.; Hansen, W. R.; Sponberg, S.; Kenny, T. W.; Fearing, R.; Israelachvili, J. N.; Full, R. J. *Proc. Natl. Acad. Sci. U. S. A.* **2002**, *99*, 12252−12256.
(29) Autumn, K.; Liang, Y. A.; Hsieh, S. T.; Zesch, W.; Chan, W. P.; Kenny, T. W.; Fearing, R.; Full, R. J. *Nature* **2000**, *405*, 681−685.
(30) Liu, K. S.; Du, J. X.; Wu, J. T.; Jiang, L. *Nanoscale* **2012**, *4*, 768−772.
(31) Vogler, E. A. *Adv. Colloid Interface Sci.* **1998**, *74*, 69−117.
(32) Guo, C. W.; Wang, S. T.; Liu, H.; Feng, L.; Song, Y. L.; Jiang, L. *J. Adhes. Sci. Technol.* **2008**, *22*, 395−402.
(33) Lafuma, a.; Quere, D. *Nat. Mater.* **2003**, *2*, 457−460.
(34) Patankar, N. A. *Langmuir* **2004**, *20*, 7097−7102.
(35) Wang, S.; Jiang, L. *Adv. Mater.* **2007**, *19*, 3423−3424.
(36) Wong, T.-S.; Sun, T. L.; Feng, L.; Aizenberg, J. *MRS Bull.* **2013**, *38*, 366−371.
(37) Ball, P. *Nature* **1999**, *400*, 507−509.
(38) Liu, X. L.; Zhou, J.; Xue, Z. X.; Gao, J.; Meng, J. X.; Wang, S. T.; Jiang, L. *Adv. Mater.* **2012**, *24*, 3401−3405.
(39) Drelich, J.; Chibowski, E. *Langmuir* **2010**, *26*, 18621−18623.
(40) Drelich, J.; Chibowski, E.; Meng, D. D.; Terpilowski, K. *Soft Matter* **2011**, *7*, 9804−9828.
(41) Zhang, L.; Zhao, N.; Xu, J. *J. Adhes. Sci. Technol.* **2014**, *28*, 769−790.
(42) Liu, K. S.; Tian, Y.; Jiang, L. *Prog. Mater. Sci.* **2013**, *58*, 503−564.
(43) Tsujii, K.; Yamamoto, T.; Onda, T.; Shibuichi, S. *Angew. Chem., Int. Ed. Engl.* **1997**, *36*, 1011−1012.
(44) Kota, A. K.; Kwon, G.; Tuteja, A. *NPG Asia Mater.* **2014**, *6*, e109.
(45) Chu, Z. L.; Seeger, S. *Chem. Soc. Rev.* **2014**, *43*, 2784−2798.
(46) Kota, A. K.; Choi, W.; Tuteja, A. *MRS Bull.* **2013**, *38*, 383−390.
(47) Tuteja, A.; Choi, W.; Ma, M. L.; Mabry, J. M.; Mazzella, S. A.; Rutledge, G. C.; McKinley, G. H.; Cohen, R. E. *Science* **2007**, *318*, 1618−1622.
(48) Tuteja, A.; Choi, W.; Mabry, J. M.; McKinley, G. H.; Cohen, R. E. *Proc. Natl. Acad. Sci. U. S. A.* **2008**, *105*, 18200−18205.
(49) Lu, Y.; Sathasivam, S.; Song, J. L.; Crick, C. R.; Carmalt, C. J.; Parkin, I. P. *Science* **2015**, *347*, 1132−1135.
(50) Xu, Z. G.; Zhao, Y.; Wang, H. X.; Wang, X. G.; Lin, T. *Angew. Chem., Int. Ed.* **2015**, *54*, 4527−4530.
(51) Kota, A. L.; Kwon, G.; Choi, W.; Mabry, J. M.; Tuteja, A. *Nat. Commun.* **2012**, *3*, 1025.
(52) Seymour, R. S.; Hetz, S. K. *J. Exp. Biol.* **2011**, *214*, 2175−2181.
(53) Wang, J. M.; Zheng, Y. M.; Nie, F. Q.; Zhai, J.; Jiang, L. *Langmuir* **2009**, *25*, 14129−14134.
(54) Chen, X.; Wu, Y. C.; Su, B.; Wang, J. M.; Song, Y. L.; Jiang, L. *Adv. Mater.* **2012**, *24*, 5884−5889.
(55) Ma, R.; Wang, J. M.; Yang, Z. J.; Liu, M.; Zhang, J. J.; Jiang, L. *Adv. Mater.* **2015**, *27*, 2384−2389.
(56) Lin, L.; Liu, M. J.; Chen, L.; Chen, P. P.; Ma, J.; Han, D.; Jiang, L. *Adv. Mater.* **2010**, *22*, 4826−4830.
(57) Xue, Z. X.; Wang, S. T.; Lin, L.; Chen, L.; Liu, M. J.; Feng, L.; Jiang, L. *Adv. Mater.* **2011**, *23*, 4270−4273.
(58) Su, B.; Wang, S. T.; Song, Y. L.; Jiang, L. *Soft Matter* **2011**, *7*, 5144−5149.
(59) Su, B.; Wang, S. T.; Song, Y. L.; Jiang, L. *Soft Matter* **2012**, *8*, 631−635.
(60) Zhang, P. C.; Wang, S. S.; Wang, S. T.; Jiang, L. *Small* **2015**, *11*, 1939−1946.
(61) Marshall, S. J.; Bayne, S. C.; Baier, R.; Tomsia, A. P.; Marshall, G. W. *Dent. Mater.* **2010**, *26*, E195−E195.
(62) Su, B.; Wang, S. T.; Song, Y. L.; Jiang, L. *Nano Res.* **2011**, *4*, 266−273.
(63) Su, B.; Wang, S. T.; Song, Y. L.; Jiang, L. *Soft Matter* **2012**, *8*, 631−635.
(64) Xue, Y. H.; Wang, H. X.; Zhao, Y.; Dai, L. M.; Feng, L. F.; Wang, X. G.; Lin, T. *Adv. Mater.* **2010**, *22*, 4814−4818.
(65) Deng, X.; Paven, M.; Papadopoulos, P.; Ye, M.; Wu, S.; Schuster, T.; Klapper, M.; Vollmer, D.; Butt, H. J. *Angew. Chem., Int. Ed.* **2013**, *52*, 11286−11289.
(66) Wooh, S.; huesmann, H.; Tahir, M. N.; Paven, M.; Wichmann, K.; Vollmer, D.; Tremel, W.; Papadopoulos, P.; Butt, H. J. *Adv. Mater.* **2015**, *27*, 7338−7343.
(67) Depecker, C.; Marzouk, H.; Trevin, S.; Devynck, J. *New J. Chem.* **1999**, *23*, 739−742.
(68) Martins, B. M.; Blaser, M.; Feliks, M.; Ullmann, G. M.; Buckel, W.; Selmer, T. *J. Am. Chem. Soc.* **2011**, *133*, 14666−14674.
(69) Lu, Z. Y.; Sun, M.; Xu, T. H.; Li, Y. J.; Xu, W. W.; Chang, Z.; Ding, Y.; Sun, X. M.; Jiang, L. *Adv. Mater.* **2015**, *27*, 2361−2366.
(70) Lu, Z. Y.; Zhu, W.; Yu, X. Y.; Zhang, H. C.; Li, Y. J.; Sun, X. M.; Wang, X. W.; Wang, H.; Wang, J. M.; Luo, J.; Lei, X. D.; Jiang, L. *Adv. Mater.* **2014**, *26*, 2683−2687.
(71) Li, Y. J.; Zhang, H. C.; Xu, T. H.; Lu, Z. Y.; Wu, X. C.; Wan, P. B.; Sun, X. M.; Jiang, L. *Adv. Funct. Mater.* **2015**, *25*, 1737−1744.
(72) Faber, M. S.; Dziedzic, R.; Lukowski, M. A.; Kaiser, N. S.; Ding, Q.; Jin, S. *J. Am. Chem. Soc.* **2014**, *136*, 10053−10061.
(73) Wu, Y. C.; Liu, K. S.; Su, B.; Jiang, L. *Adv. Mater.* **2014**, *26*, 1124−1128.
(74) Wang, S. S.; Wu, Y. C.; Kan, X. N.; Su, B.; Jiang, L. *Adv. Funct. Mater.* **2014**, *24*, 7007−7013.
(75) Hatton, B. D.; Aizenberg, J. *Nano Lett.* **2012**, *12*, 4551−4557.
(76) Mishchenko, L.; Khan, M.; Aizenberg, J.; Hatton, B. D. *Adv. Funct. Mater.* **2013**, *23*, 4577−4584.
(77) Aebisher, D.; Bartusik, D.; Liu, Y.; Zhao, Y. Y.; Barahman, M.; Xu, Q. F.; Lyons, A. M.; Greer, A. *J. Am. Chem. Soc.* **2013**, *135*, 18990−18998.
(78) Zhao, Y. Y.; Liu, Y.; Xu, Q. F.; Barahman, M.; Bartusik, D.; Greer, A.; Lyons, A. M. *J. Phys. Chem. A* **2014**, *118*, 10364−10371.
(79) Lei, Y. J.; Sun, R. Z.; Zhang, X. C.; Feng, X. J.; Jiang, L. *Adv. Mater.* **2015**, DOI: 10.1002/adma.201503520.
(80) Wang, X. L.; Liu, X. J.; Zhou, F.; Liu, W. M. *Chem. Commun.* **2011**, *47*, 2324−2326.
(81) Wong, T. S.; Kang, S. H.; Tang, S. K. Y.; Smythe, E. J.; Hatton, B. D.; Grinthal, A.; Aizenberg, J. *Nature* **2011**, *477*, 443−447.
(82) Epstein, A. K.; Wong, T. S.; Belisle, R. A.; Boggs, E. M.; Aizenberg, J. *Proc. Natl. Acad. Sci. U. S. A.* **2012**, *109*, 13182−13187.
(83) Yao, X.; Hu, Y. H.; Grinthal, A.; Wong, T. S.; Mahadevan, L.; Aizenberg, J. *Nat. Mater.* **2013**, *12*, 529−534.
(84) Cui, J. X.; Daniel, D.; Grinthal, A.; Lin, K. X.; Aizenberg, J. *Nat. Mater.* **2015**, *14*, 790−795.
(85) Hou, X.; Hu, Y. H.; Grinthal, A.; Khan, M.; Aizenberg, J. *Nature* **2015**, *519*, 70−73.
(86) Liu, H. L.; Zhang, P. C.; Liu, M. J.; Wang, S. T.; Jiang, L. *Adv. Mater.* **2013**, *25*, 4477−4481.
(87) Zhang, P. C.; Liu, H. L.; Meng, J. X.; Yang, G.; Liu, X. L.; Wang, S. T.; Jiang, L. *Adv. Mater.* **2014**, *26*, 3131−3135.

DOI: 10.1021/jacs.5b12728
J. Am. Chem. Soc. 2016, 138, 1727−1748

(88) Yao, X.; Ju, J.; Yang, S.; Wang, J. J.; Jiang, L. *Adv. Mater.* **2014**, *26*, 1895−1900.
(89) Ding, Y.; Zhang, J. J.; Zhang, X. Q.; Zhou, Y. H.; Wang, S. T.; Liu, H. L.; Jiang, L. *Adv. Mater. Interfaces* **2015**, *2*, 1500177.
(90) Huang, Y.; Zhou, J. M.; Su, B.; Shi, L.; Wang, J. X.; Chen, S. R.; Wang, L. B.; Zi, J.; Song, Y. L.; Jiang, L. *J. Am. Chem. Soc.* **2012**, *134*, 17053−17058.
(91) Kuang, M. X.; Wang, J. X.; Bao, B.; Li, F. Y.; Wang, L. B.; Jiang, L.; Song, Y. L. *Adv. Opt. Mater.* **2014**, *2*, 34−38.
(92) Su, B.; Wang, S. T.; Ma, J.; Song, Y. L.; Jiang, L. *Adv. Funct. Mater.* **2011**, *21*, 3297−3307.
(93) Krumpfer, J. W.; McCarthy, T. J. *J. Am. Chem. Soc.* **2011**, *133*, 5764−5766.
(94) Su, B.; Wang, S. T.; Ma, J.; Wu, Y. C.; Chen, X.; Song, Y. L.; Jiang, L. *Adv. Mater.* **2012**, *24*, 559−564.
(95) Wu, Y. C.; Su, S.; Jiang, L. *ACS Nano* **2012**, *6*, 9005−9012.
(96) Wu, Y. C.; Chen, X.; Su, B.; Song, Y. L.; Jiang, L. *Adv. Funct. Mater.* **2012**, *22*, 4569−4576.
(97) Xin, Z. Q.; Su, B.; Wang, J. J.; Zhang, X. Y.; Zhang, Z. L.; Deng, M. M.; Song, Y. L.; Jiang, L. *Small* **2013**, *9*, 722−726.
(98) Jiang, X. Y.; Wu, Y. C.; Su, B.; Xie, R. G.; Yang, W. S.; Jiang, L. *Small* **2014**, *10*, 258−264.
(99) Su, B.; Wang, S. T.; Wu, Y. C.; Chen, X.; Song, Y. L.; Jiang, L. *Adv. Mater.* **2012**, *24*, 2780−2785.
(100) Wu, Y.; Bao, B.; Su, B.; Jiang, L. *J. Mater. Chem. A* **2013**, *1*, 8581−8586.
(101) Wu, Y. C.; Su, B.; Jiang, L.; Heeger, A. J. *Adv. Mater.* **2013**, *25*, 6526−6533.
(102) Su, B.; Wu, Y. C.; Tang, Y.; Chen, Y.; Cheng, W. L.; Jiang, L. *Adv. Mater.* **2013**, *25*, 3968−3972.
(103) Su, B.; Zhang, C.; Chen, S. R.; Zhang, X. Y.; Chen, L. F.; Wu, Y. C.; Nie, Y. W.; Kan, X. N.; Song, Y. L.; Jiang, L. *Adv. Mater.* **2014**, *26*, 2501−2507.
(104) Kan, X. N.; Su, B.; Jiang, L. *Small* **2014**, *10*, 2570−2577.
(105) Wu, Y. C.; Feng, J. G.; Jiang, X. Y.; Zhang, Z.; Wang, X. D.; Su, B.; Jiang, L. *Nat. Commun.* **2015**, *6*, 6737.
(106) Ma, C. D.; Wang, C. X.; Acevedo-Vélez, C.; Gellman, S. H.; Abbott, N. L. *Nature* **2015**, *517*, 347−350.
(107) Garde, S. *Nature* **2015**, *517*, 277−278.
(108) Liu, X. K.; Leng, C.; Yu, L.; He, K.; Brown, L. J.; Chen, Z.; Cho, J. H.; Wang, D. Y. *Angew. Chem., Int. Ed.* **2015**, *54*, 4851−4856.
(109) Liu, M. J.; Xue, Z. X.; Liu, H.; Jiang, L. *Angew. Chem., Int. Ed.* **2012**, *51*, 8348−8351.
(110) Cheng, Z. J.; Lai, H.; Du, Y.; Fu, K. W.; Hou, R.; Zhang, N. Q.; Sun, K. N. *ACS Appl. Mater. Interfaces* **2013**, *5*, 11363−11370.
(111) Cheng, Z. J.; Lai, H.; Du, Y.; Fu, K. W.; Hou, R.; Li, C.; Zhang, N. Q.; Sun, K. N. *ACS Appl. Mater. Interfaces* **2014**, *6*, 636−641.
(112) Quere, D. *Annu. Rev. Fluid Mech.* **2013**, *45*, 197−215.
(113) Zhang, T.; Wang, J. M.; Chen, L.; Zhai, J.; Song, Y. L.; Jiang, L. *Angew. Chem., Int. Ed.* **2011**, *50*, 5311−5314.
(114) Kim, H.; Truong, B.; Buongiorno, J.; Hu, L. W. *Appl. Phys. Lett.* **2011**, *98*, 083121.
(115) Bernardin, J. D.; Mudawar, I. *J. Heat Transfer* **1999**, *121*, 894−903.
(116) Liu, C. C.; Ju, J.; Ma, J.; Zheng, Y. M.; Jiang, L. *Adv. Mater.* **2014**, *26*, 6086−6091.
(117) Parker, A. R.; Lawrence, C. R. *Nature* **2001**, *414*, 33−34.
(118) Liu, C. C.; Ju, J.; Zheng, Y. M.; Jiang, L. *ACS Nano* **2014**, *8*, 1321−1329.
(119) Zheng, Y. M.; Bai, H.; Huang, Z. B.; Tian, X. L.; Nie, F. Q.; Zhao, Y.; Zhai, J.; Jiang, L. *Nature* **2010**, *463*, 640−643.
(120) Ju, J.; Bai, H.; Zheng, Y. M.; Zhao, T. Y.; Fang, R. C.; Jiang, L. *Nat. Commun.* **2012**, *3*, 1247.
(121) Li, K.; Ju, J.; Xue, Z.; Ma, J.; Feng, L.; Gao, S.; Jiang, L. *Nat. Commun.* **2013**, *4*, 2276.
(122) Bai, H.; Ju, J.; Zheng, Y. M.; Jiang, L. *Adv. Mater.* **2012**, *24*, 2786−2791.
(123) Hou, Y. P.; Gao, L. C.; Feng, S. L.; Chen, Y.; Xue, Y.; Jiang, L.; Zheng, Y. M. *Chem. Commun.* **2013**, *49*, 5253−5255.
(124) Chen, Y.; Wang, L.; Xue, Y.; Zheng, Y. M.; Jiang, L. *Soft Matter* **2012**, *8*, 11450−11454.
(125) Chen, Y.; Wang, L.; Xue, Y.; Jiang, L.; Zheng, Y. M. *Sci. Rep.* **2013**, *3*, 2927.
(126) Bai, H.; Tian, X. L.; Zheng, Y. M.; Ju, J.; Zhao, Y.; Jiang, L. *Adv. Mater.* **2010**, *22*, 5521−5525.
(127) Zhang, H. C.; Hou, X.; Zeng, L.; Yang, F.; Li, L.; Yan, D. D.; Tian, Y.; Jiang, L. *J. Am. Chem. Soc.* **2013**, *135*, 16102−16110.
(128) Liu, M. Y.; Zhang, H. C.; Li, K.; Heng, L. P.; Wang, S. T.; Tian, Y.; Jiang, L. *Adv. Funct. Mater.* **2015**, *25*, 421−426.
(129) Hou, X.; Guo, W.; Jiang, L. *Chem. Soc. Rev.* **2011**, *40*, 2385−2401.
(130) Wen, L. P.; Tian, Y.; Ma, J.; Zhai, J.; Jiang, L. *Phys. Chem. Chem. Phys.* **2012**, *14*, 4027−4042.
(131) Guo, W.; Tian, Y.; Jiang, L. *Acc. Chem. Res.* **2013**, *46*, 2834−2846.
(132) Tian, Y.; Jiang, L. *Sci. China: Chem.* **2011**, *54*, 603−610.
(133) Hou, X.; Guo, W.; Xia, F.; Nie, F. Q.; Dong, H.; Tian, Y.; Wen, L. P.; Wang, L.; Cao, L. X.; Yang, Y.; Xue, J. M.; Song, Y. L.; Wang, Y. G.; Liu, D. S.; Jiang, L. *J. Am. Chem. Soc.* **2009**, *131*, 7800−7805.
(134) Guo, W.; Xia, H. W.; Xia, F.; Hou, X.; Cao, L. X.; Wang, L.; Xue, J. M.; Zhang, G. Z.; Song, Y. L.; Zhu, D. B.; Wang, Y. G.; Jiang, L. *ChemPhysChem* **2010**, *11*, 859−864.
(135) Tian, Y.; Zhang, Z.; Wen, L.; Ma, J.; Zhang, Y.; Liu, W.; Zhai, J.; Jiang, L. *Chem. Commun.* **2013**, *49*, 10679−10681.
(136) Hou, X.; Yang, F.; Li, L.; Song, Y. L.; Jiang, L.; Zhu, D. B. *J. Am. Chem. Soc.* **2010**, *132*, 11736−11742.
(137) Wen, L. P.; Hou, X.; Tian, Y.; Zhai, J.; Jiang, L. *Adv. Funct. Mater.* **2010**, *20*, 2636−2642.
(138) Guo, W.; Cao, L. X.; Xia, J. C.; Nie, F. Q.; Ma, W.; Xue, J. M.; Song, Y. L.; Zhu, D. B.; Wang, Y. G.; Jiang, L. *Adv. Funct. Mater.* **2010**, *20*, 1339−1344.
(139) Gao, J.; Guo, W.; Feng, D.; Wang, H.; Zhao, D.; Jiang, L. *J. Am. Chem. Soc.* **2014**, *136*, 12265−12272.
(140) Guo, W.; Cheng, C.; Wu, Y.; Jiang, Y.; Gao, J.; Li, D.; Jiang, L. *Adv. Mater.* **2013**, *25*, 6064−6068.

DOI: 10.1021/jacs.5b12728
J. Am. Chem. Soc. 2016, 138, 1727−1748